Synthetic Creation of a Chemotactic System via Utilization of Magnetically Actuated Microrobotic Walkers

by

Joshua Paul Steimel

Submitted to the Department of Materials Science and Engineering in Partial Fulfillment of the Requirements for the Degree of

Bachelor of Science

at the

Massachusetts Institute of Technology

May 2012
[JUNE 2012]

Signature of Author.....
Department of Materials Science and Engineering
May 4, 2012

Certified by.....
Alfredo Alexander-Katz
Professor of Materials Science and Engineering
Thesis Supervisor

Accepted by.....
Jeffrey C. Grossman
Professor of Materials Science and Engineering
Chair, Undergraduate Committee

Synthetic Creation of a Chemotactic System via Utilization of Magnetically Actuated Microrobotic Walkers

by

Joshua Paul Steimel

Submitted to the Department of Materials Science and Engineering on May 4th, 2012 in Partial Fulfillment of the Requirements for the Degree of Bachelor of Science

Abstract

Chemotaxis is a fundamental biological process that plays an important role in disease, reproduction, and most biological functions. Here, we present a radically novel method to create the first synthetic chemotactic system which utilized magnetically actuated microrobotic walkers. The system used a rotating magnetic field that once actuated induced the magnetic beads to self-assemble into microrobots and walk on surfaces. The velocity of these microrobotic walkers could be modulated by the frequency and the number of beads that composed the walkers. The receptor-ligand pair of biotin-streptavidin was utilized due to the extremely strong binding affinity of the pair. The presence of free biotin binding sites on the surface was required to obtain chemotactic motion as these binding sites modulated walker velocity. The walkers moved faster in areas with a high density of binding sites and slower in areas with a low density of binding sites. To achieve chemotaxis, gradients in the density of binding sites were required. Gradients were created by placing a droplet of concentrated streptavidin on a biotynlated slide and letting the droplet evaporate. The Gaussian evaporation process created differentials in the density of binding sites. A series of continuous velocity measurements were conducted across the sample to map the walker velocity profile. The velocity profile illustrated regions with a high density of binding sites as well as a local minimum in the density of binding sites. The discrete motion of the beads was analyzed to understand how chemotactic directed motion could be achieved by breaking the symmetry of the system. Walkers in an area with a high density of binding sites experienced a significant amount of "sticking" followed by hinge-like motion, while walkers in a low density area exhibited virtually no "sticking" and tended to slip much more frequently. Walkers were then placed on a random walk path and chemotactic directed motion was observed as the walkers drifted towards regions with a high density of binding sites. The drift velocities that were extracted from the random walk path illustrated the discrepancy between the chemical gradients present in this synthetic chemotactic system.

Keywords: biomimetic, chemotaxis, superparamagnetic microrobotic walkers, biotin, streptavidin, PEG, drift velocity, random walk,

Thesis Supervisor: Alfredo Alexander-Katz

Title: Professor of Materials Science and Engineering

Table of Contents

Chapter 1: Introduction.....8

Chapter 2: Creating Self-Assembled Microrobotic Walkers.....12

I. Introduction.....**12**
A. Synthetically Mimicking Ciliary Propulsion and Molecular Motors via Microrobotic Walkers.....12

II. Methods.....**15**
A. Bead Choice and Sample Preparation.....15
B. Imaging, Actuation, and Characterization.....18
C. Investigating Superparamagnetism.....20

III. Results and Discussion.....**21**
A. Walker Velocity Increases Linearly as Chain Length Increases.....21
B. Walker Velocity Increases Linearly as Hz Increases for Fixed Chain Lengths.....22
C. Solulink Beads Exhibit Some Finite Coercivity and Paramagnetism.....23

IV. Conclusion.....**25**

Chapter 3: Creating a Chemotactic Environment.....27

I. Introduction.....**27**
A. Benefit of Ligand-Receptor Synthetic Chemotaxis Approach.....27
B. Chemotactic System: Utilization of the Biotin-Streptavidin Bond and Solulink Bead Functionalization Using Biotin-PEG.....28

II. Methods.....**30**
A. Droplet Method for Gradient Creations/Sample Preparation.....30

B. Velocity Measurement Protocol.....32
C. PEG Binding Calibration.....33

III. Results and Discussion.....33
A. Biotin-PEG Binding Saturation Of Solulink Beads Occurs After Incubation Period of 20 Minutes at 25°C.....34
B. Velocity Profile of Sample Illustrates High and Low Density Areas of Biotin Binding Sites.....35

IV. Conclusion.....37

Chapter 4: Breaking Symmetry: Further Evidence of a Chemotactic System.....39

I. Introduction.....39
A. A Closer Look at Chemotactic Movement Dynamics: Chemotactic Drift.....39

II. Methods.....39
A. Intensive Motion Analysis Across Gradient.....40
B. Applying a Random Walk/Monte Carlo Method to Investigate Chemotactic Motion.....40
C. "Back-and-Forth" Protocol to Derive Drift Force/Velocity.....41

III. Results and Discussion.....42
A. Symmetry is Broken By Time Lag at Areas with a High Density of Biotin Binding Sites.....42
B. Beads Exhibit Chemotactic Directed Motion Via Aggregation at Areas with a High Density of Binding Sites.....45
C. Two Distinct Drift Velocities Illustrate Chemotaxis and Differences in Density of Biotin Binding Sites.....48

IV. Conclusion.....51

Chapter 5: Conclusions and Future Work.....52

References.....55

Acknowledgements.....59

Appendix: Frequency and Walk Duration Effect on Chemotactic System.....60

Appendix: Gradient Quantification.....63

Appendix: Dendritic Formation.....65

Appendix: Effect of Temperature and Salt Concentration on PEG Phase Transition.....66

List of Figures

Figure 1: Modes of Cellular Transport.....12

Figure 2: Attempts to Synthetically Mimic Cellular Motion.....13

Figure 3: Schematic of Microrobotic Walker Motion and Interaction with Surface.....14

Figure 4: Solulink Superparamagnetic Beads.....15

Figure 5: Schematic of Channel Set-Up.....17

Figure 6: Schematic of Proposed Experimental Set-Up.....19

Figure 7: Visualization of Experimental Set-Up.....20

Figure 8: Velocity of Walkers as the Number of Beads Increases.....22

Figure 9: Velocity of Walkers Increases as Hz Increases.....23

Figure 10: Hysteresis Loop Generated by VSM.....24

Figure 11: Solulink Beads Exhibit Finite Hysteresis Loop.....25

Figure 12: Schematic of the Biotin-Streptavidin Binding Complex.....27

Figure 13: Schematic of Walker Motion as a Function of Binding Site Density...28

Figure 14: Schematic of Masking Protocol.....29

Figure 15: Water Contact Angle Measurements on Biotin Surface After Streptavidin Exposure.....31

Figure 16: Biotin-PEG Calibration for Optimal Solulink Bead Coverage for Masking Protocol.....34

Figure 17: Velocity Profile of Sample.....36

Figure 18: Distance Traveled as a Function of Sample Distance.....43

Figure 19: Time Walker Traveled as a Function of Sample Distance.....44

Figure 20: "Short" Random Walk Histogram.....46

Figure 21: "Long" Random Walk Histogram.....48

Figure 22: Drift Velocity of Walkers Drifting Toward the 0μm Region.....49

Figure 23: Drift Velocity of Walkers Drifting Toward the 800μm Region.....50

Figure 24: Walker Distance Traveled at 5Hz in Both Directions.....60

Figure 25: Walker Velocity at 5Hz in Both Directions.....61

Figure 26: Walker "Short" Random Walk Histogram as Walk Duration Increases.....62

Figure 27: Confocal Microscopy Images.....63

Figure 28: Dendritic Formation Images.....65

Figure 29: PEG Phase Diagram.....66

Chapter 1: Introduction

The basis of life as we know it is the continuous search for chemical energy and the subsequent conversion of that chemical energy into motion. All biological systems, ranging from the molecular to the cellular scale, must perform these tasks and the dynamics of these systems are known to be governed by out of equilibrium laws.[1,2] This basic necessity for survival requires that organisms must have some facility that allows them to detect and respond to changes in the environment. A number of mechanisms have evolved by which organisms sense their environment and respond to signals they detect. The typical response involves movement toward favorable environmental signals and away from a potentially toxic environment. This movement can involve a process called kinesis, which is a change in velocity or a change in the frequency of turning by the organism in a particular environment. Organisms may also utilize a movement response called taxis, which is a directed movement toward or away from a particular environment. Additionally an organism's response may also involve a combination of these two processes.

In the field of biomimetics, designing functional assemblies or molecules that can mimic these biological systems and processes is vital in order to understand how to replicate such systems for applications that are similar to their biological function, and even more so for applications that depart from their biological counterparts. Perhaps one of the most remarkable and synthetically desirable properties of some biological cellular systems is the process known as chemotaxis.[3,4] In the chemotactic process, a cell is able to detect the concentration gradient of a particular chemical signal in an environment and then moves accordingly to that gradient. Numerous types of biological cells exhibit this process, which only serves to exponentially increase the possible applications if one could synthetically mimic chemotaxis. For example,

bacterial E.Coli uses chemotaxis (manifested in the stumble and run motion) in order to move towards regions that are rich in nutrients or to avoid regions of high toxicity.[3-10] Spermatozoa chemotaxis during fertilization is also widely observed. The spermatozoa swimming is directed toward an unfertilized egg based on a concentration gradient of sperm activating and attracting factor (SAAF) and Ca^{2+} ions which modulates flagellar beating as well as swimming direction.[11] Additionally, neutrophils, a type of white blood cell involved in combating infections, can detect chemicals (specifically cytokines) that are produced by pathogens in a wound. They migrate toward this "smell" in order to kill the pathogen via phagocytosis (ingestion), the release of soluble anti-microbials, or the generation of neutrophil extracellular traps (NETs).[4,12-15]

As of yet, microscopic machines or robots that can mimic such behavior have not been realized. However, such microrobots would clearly be of interest because they would not only be able to sense the presence of chemical agents but also identify the source of these agents. The potential applications for synthetically created microrobotic chemotactic systems are immense and varied. Such systems could allow in-situ characterization of surface fouling. We could learn how different surface types interact hydrodynamically and chemically under diverse aqueous conditions and how this could affect the long-term performance of coatings on aquatic equipment. The recent findings that chemotaxis seems to be inextricably related to many diseases opens the door to future applications for these microrobotic devices and systems in diagnosing and treating human diseases.

Here, we propose to explore a new and radical approach to designing chemotactic microscopic robots by exploiting the coupling between synthetic (or biological) surfaces and functionalized superparamagnetic particles or beads. Our microrobotic walkers are composed of

chains (or rods) of superparamagnetic beads that self-assemble due to magnetic forces. In order to make these superparamagnetic microrobotic walkers (referred to as "walkers" henceforth) walk, a rotating magnetic field was used to drive the chains to turn and walk on surfaces. The first set of experiments aimed to develop a protocol that would force these walkers to walk across the surface of an uncoated glass slide. Ideally without the walkers getting stuck or exhibiting some gradient in velocity due to the roughness of the slide (or some other non-specific interactions between the walkers and the slide). We illustrated that the velocity of the walkers linearly increase as beads are added to the walker chain and as the frequency of turns increases. Coercivity measurements were also made in order to show that the beads weren't truly superparamagnetic, explaining why a single bead exhibited a non-negligible velocity.

The next set of experiments designed and tested a chemotactic system using functionalized walkers and a coated surface. The biological receptor-ligand pair of biotin and streptavidin was utilized to control the coupling between the walkers and the coated surface, due to the extremely high binding affinity between biotin and streptavidin (the strongest noncovalent biological interaction known), on the order of 80kT.[16] The idea was to utilize this bond to observe net motion in the direction of a gradient. Walkers should move toward a region with a high density of biotin binding sites and away from regions with a low density of biotin binding sites. The surface in this chemotactic system was a glass slide with a biotynlated surface and the gradient was created by inserting a droplet of concentrated streptavidin which was allowed to evaporate and bind to the free biotin sites. This created a gradient in the density of biotin binding sites. The walkers were functionalized with a biotin-PEG polymer brush. Our theoretical framework was confirmed by measuring the continuous velocity profile of the walkers across the surface, with the velocity being larger at areas with a high density of free biotin binding sites. In

order to observe chemotactic directed motion towards the gradient, the walkers were made to do random walks across the surface. Furthermore, a systematic analysis of the walker motion during these random walks allowed us to derive a drift force or drift velocity term. This, in conjunction with the previous data demonstrated that we had successfully created the first synthetic chemotactic system.

Chapter 2: Creating Self-Assembled Microrobotic Walkers

I. Introduction

A. Synthetically Mimicking Ciliary Propulsion and Molecular Motors via Microrobotic Walkers

Nature has devised a number of mechanisms to transport materials at the cellular level. However, at microscopic length scales, where inertia becomes irrelevant, any type of cyclic motion will lead to a net translation of zero. Therefore, mechanisms of translation must break the symmetry of the system in order to translate. Of the numerous modes of transportation available at the cellular level, perhaps the two most prominent are flagellar rotation and ciliary beating. In the ciliary mode of transport, the filaments are anchored to the surface of the cell but the filaments remain flexible, allowing for modulation in filament beating. The velocity is thusly dependent on filament deformation. The symmetry in this system is therefore broken due to the flexibility of the filaments. Flagellar motion breaks the symmetry of the system by utilizing its characteristic spiral filament which functions much like a corkscrew. When the filament undulates, it provides the primary locomotion mechanism for the cell to move, as seen in Figure 1.

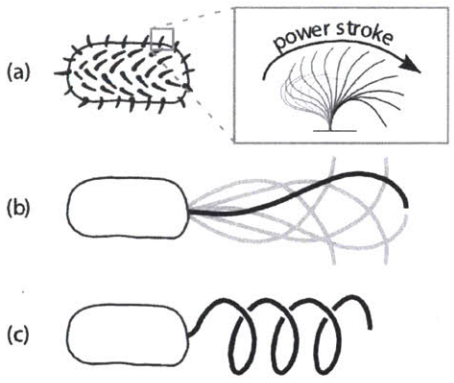

Figure 1: a) A depiction of the ciliary mode of cellular transportation. Particularly, how the flexibility of the filaments and speed of the power stroke breaks the symmetry in the system and allows for transport. b) A depiction

of flagellar motion and c) a typical flagellar beating in a corkscrew type motion, breaking the symmetry of the system.[17]

Synthetically mimicking cellular propulsion mechanisms has received significant attention in the past decades and a number of advances have been made in designing artificial swimmers that use different locomotion schemes at the micro and even nano scale.[18] Designs for propulsion at the microscopic scale range from artificial flagella swimmers that are activated by the application of a magnetic field[19-23], phoretic swimmers that rely on the catalysis of a reaction on one side of the swimmer which causes a pressure differential and subsequent propulsion[24-27], electrical micro-machined "real-robotic swimmers"[28], and the walkers that we used[29-34], all of which can be seen in Figure 2.

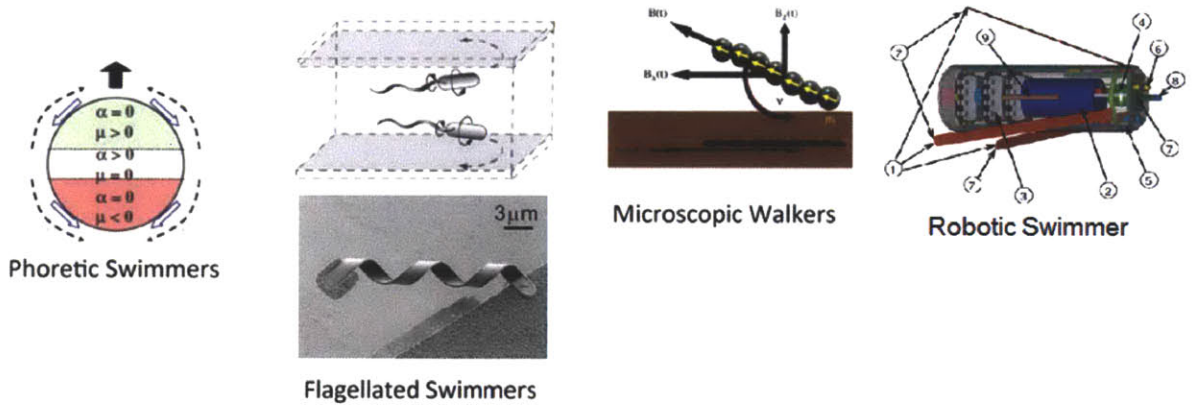

Figure 2: A small sample of the numerous different synthetic attempts to mimic cellular motion.[17,28]

The walkers we chose for this project have several distinct advantages over the numerous other transport devices. Our walkers are essentially a hybrid between biological cilia or flagella, used to propel fluids and organisms, and molecular motors, which transport cargo inside the cells. This dual functionality isn't trivial. Molecular motors are essentially proteins that move on cytoskeleton tracks due to the binding affinity of the motor "feet" to the track. This binding affinity function creates enhanced friction near the surface of the track. Without this binding affinity, these motors would simply continue to slip without translating. This walking ability of

the "molecular motor" aspect of these walkers (in addition to the walker motion closely resembling cilia and flagellar fluid propulsive properties which have been well documented in theories applied to cilia carpets[35-39] also see Chapter 5: Conclusion and Future Work), make our walkers extremely unique and best suited to the task of synthetically mimicking chemotaxis.

Another unique aspect of our walkers is their spontaneous self-assembly upon application of a magnetic field. As seen in Figure 3, the superparamagnetic beads are initially unconnected.

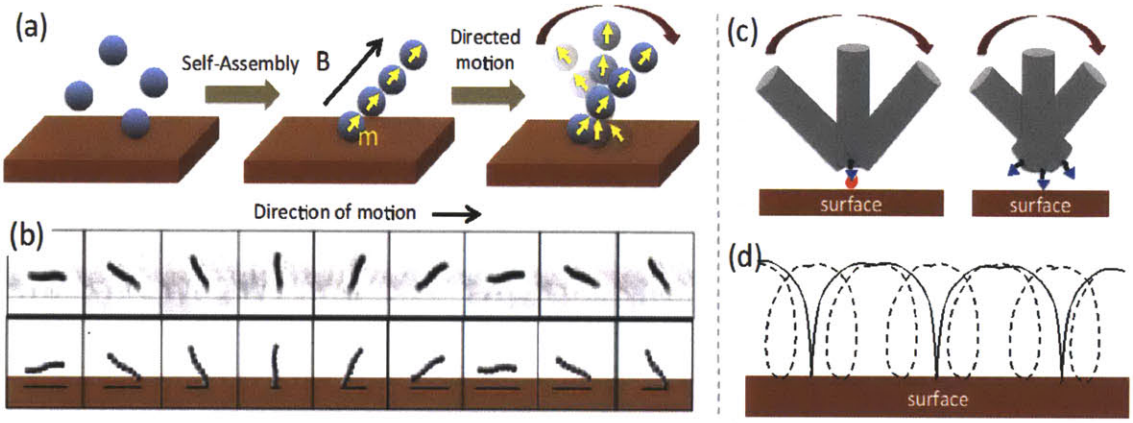

Figure 3: Schematic of walkers. (a) A group of superparamagnetic particles self-assembles into a microscopic machine in the presence of a magnetic field B because each particle acquires a magnetic moment *m*. Upon rotation of the field, the chain starts walking on surfaces seen experimentally (upper trace b) and in simulations (lower trace b). (c) The velocity of the walker can be tuned via the coupling of the surface and the beads represented by the existence (or not) of complementary "binding" sites (red dot). For strong friction (high binding strength), one expects a hinge type rapid motion (solid trace of one of the ends of the chain) while if the system slips, the resulting velocity is lower (dashed trace). By controlling the surface-bead interactions, we can control the velocity of the robots and detect inhomogeneous patterns on surfaces effectively creating a chemotactic microscopic robot.

Upon application of a magnetic field, the beads spontaneously self-assemble as each bead acquires a magnetic moment. As the field rotates, the chains or rotors, will start to walk along the surface. This type of motion allows the velocity to be tuned by coupling the functionalized beads to a surface that has binding sites. When the chain encounters a binding site (the red dot in

Figure 3), the chain will exhibit a rapid hinge-like motion. If there is no binding site, the chain will slip and move at a significantly lower velocity. These walkers are ideal for synthetically mimicking chemotaxis since the surface and the beads can be functionalized to achieve strong coupling and obtain directed motion. But before this could be achieved, the beads must be able to walk on an uncoated glass slide surface, their velocity only being tunable by increasing the number of beads in a chain or increasing the frequency of turns.

II. Methods

A. Bead Choice and Sample Preparation

In order to construct our walkers, in addition to the beads having some magnetic affinity, the beads need to be suited to functionalization. Additionally, the size of the beads had to be chosen so that they could be easily imaged by our experimental set-up (40X objective). To accomplish this, superparamagnetic beads were purchased from Solulink as seen in Figure 4.

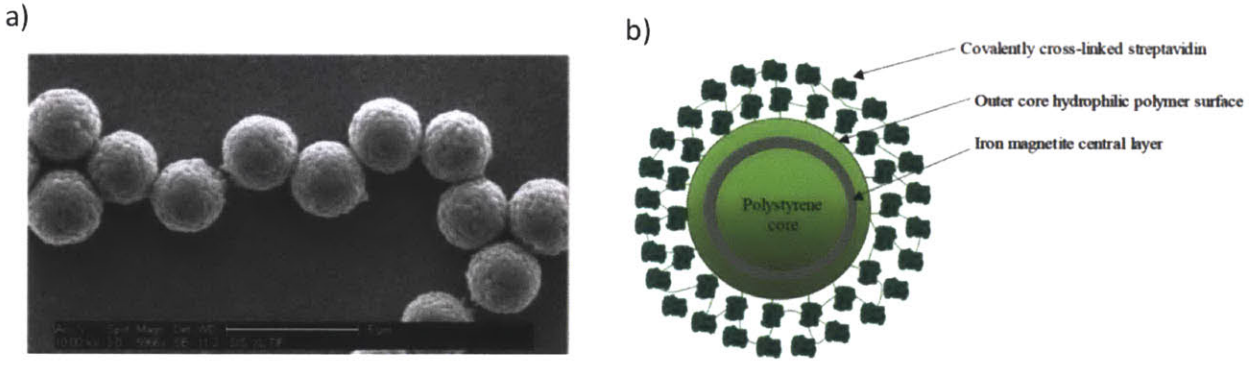

Figure 4: Superparamagnetic beads purchased from Solulink. An SEM image shows the covalently cross-linked streptavidin covering the polystyrene core and iron magnetite central layer in a). b) A schematic of the superparamagnetic bead structure.

In order to synthetically mimic chemotaxis, we wanted to utilize the high binding affinity of the biotin-streptavidin bond. Thus, one of our main priorities was accomplished by purchasing these beads as the polystyrene core and iron magnetite central layer is coated with covalently cross-linked streptavidin which can be further functionalized with a biotin-PEG polymer brush.

Solulink offers these beads in two different sizes, 0.8μm and 2.8μm. Both exhibit excellent "walking behavior," but it was difficult to differentiate a "dimer" walker (2 beads in a chain) vs. a "trimer" walker (3 beads in a chain) for the 0.8μm size. The 2.8μm beads were utilized since they were better suited for the optical limitations of our experimental set-up. Invitrogen makes the same polystyrene beads with a streptavidin functionalized surface, the size of the beads are1μm. They also exhibit the same walking behavior, but are also able to reversibly assemble and disassemble. The Solulink beads, on the other hand, don't readily disassemble without some manipulation of the magnetic field or application of a generous polymer brush (the steric hindrance of the brush seems to force the beads apart). The lack of reversibility that the Solulink beads exhibit is probably due to their method of covalently cross-linking streptavidin on the surface of the polystyrene beads. When these beads assemble upon actuation of a magnetic field, we hypothesized that the cross-linked streptavidin would become entangled between beads, preventing disassociation when the magnetic field is removed. However, this is of little consequence to our purposes and was actually beneficial when running our random walk tests as the beads didn't drift off when they disassembled, giving us greater control and precision over the walkers.

Proper sample preparation was of integral importance to successfully creating a synthetic chemotactic system. And clever sample preparation was even required to get the walkers to move on a glass slide. For this set of experiments on an uncoated glass slide, a rigorous cleaning process was needed to minimize the number of beads that stuck to the glass slide due to various non-specific interactions. Each glass slide purchased from Xenopore was sonicated in an aqueous solution for approximately twenty minutes. The slide was rinsed with water and then a generous spritz of Windex was applied to the glass slide. The surfactants in the Windex solution

seem to have a significant effect in reducing the number of beads sticking to the surface. The same effect was seen if soap was introduced into the solution of beads and phosphate buffer. However, introducing the soap into the solution was extremely problematic and troublesome, making Windex the superior alternative. The slide was dried with the Kimwipes and rinsed once more with water and cleaned with Windex.

The next step was the creation of "channels." Two lines of 3M double-sided tape were placed on the slide, as seen in Figure 5, to create a channel of approximately 5mm in width.

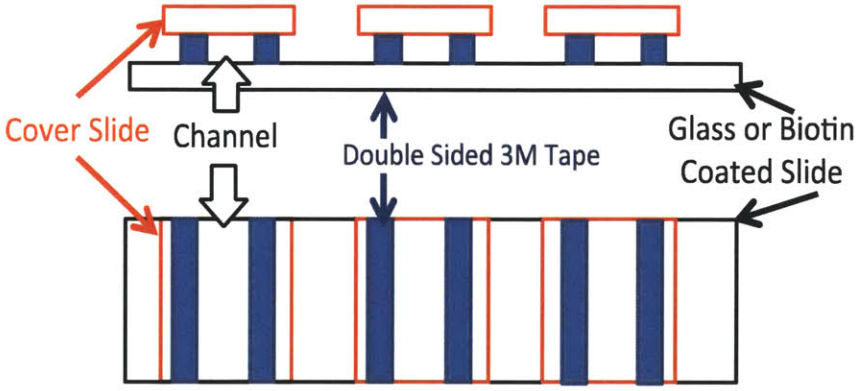

Figure 5: Side view (the top) and top view (the bottom) of the sample channels used for imaging and actuation.

A coverslip that had undergone the same water and Windex cleaning procedure was placed on top of the tape to create the channel. The solution of beads and phosphate buffer that had been previously prepared in smaller vials prior to the channel creation was now injected into the channel via a micropipette. When the solution was injected into the channels it was instantaneously sucked into the channel due to capillary forces. The entire sample was then placed onto the sample stage of our experimental apparatus, ready to be magnetically actuated. After which, the samples were discarded.

In preparing the solutions to be injected into the channels, there were two main objectives that had to be met. First, we noticed that after the bead solution had been extracted from the

Solulink package and placed in separate vials for several weeks, there was a significant amount of bead aggregation. Since these beads don't disassemble easily, we needed to get rid of this aggregation. Also, we had to find the dilution that would give us a suitable density of robots so that we could ensure that the velocity of the beads was their true velocity (i.e. any added velocity due to the effective flow generated by the other walkers had to be eliminated). Several attempts were made to prevent bead aggregation including shining a heat lamp on the solution for five to ten minutes, placing a magnet at the bottom of the solution to pull huge aggregates to the bottom of the vial and then extract the beads at the top of the solution, and even making extremely dilute solutions in the hopes of minimizing aggregation. Eventually, we adopted the protocol of vortexing all bead solutions for approximately three to five minutes before injection into the channels. This eliminated virtually all traces of aggregation, allowing us to selectively assemble the desired walker length for motion analysis. In order to find the correct dilution for analysis, we simply examined the relative density of walkers per 150μmx150μm area and analyzed several "one bead walker" velocities. We found that the appropriate dilution so that flow induced velocity could be neglected, was approximately a 1:100 ratio of beads to phosphate buffer solution before insertion into the sample. Approximately 40-50μL of solution was inserted to fully saturate the channel.

B. Imaging, Actuation, and Characterization

The essential experimental apparatus utilized for the rest of the experiments will henceforth be referred to as simply "the apparatus." A schematic of which can be seen below in Figure 6.

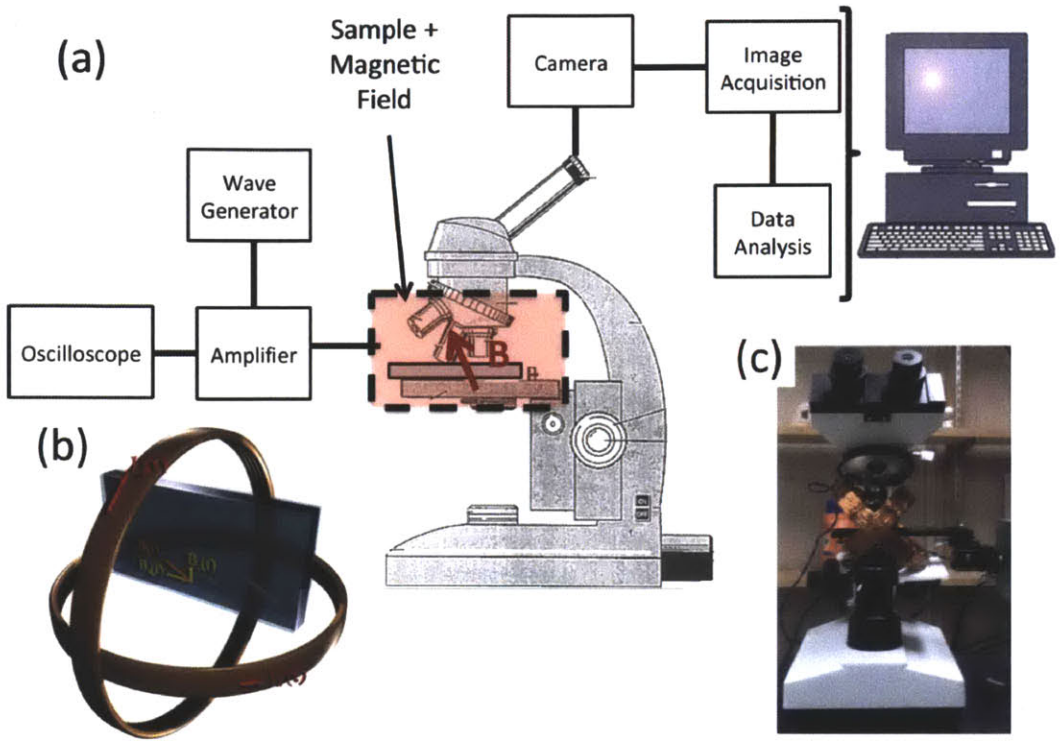

Figure 6: Schematic of the proposed experimental set-up. (a) Diagram of the experimental set-up. (b) Visualization of the rotating magnetic field that is generated by the pair of orthogonal coils that permits walker movement. (c) Close-up view of the current microscope, sample stage, and coil set-up.

The apparatus consisted of a light microscope with mounted Helmholtz coils centered on the sample to produce rotating magnetic fields. A wave generator ran two sinusoidal signals (one per coil), phase shifted by 90 degrees, to obtain a homogenous rotating magnetic field. The relatively small coils were chosen so that the Helmholtz coils would fit within the objective and the condenser in order to avoid any unwanted magnetic eddies that could be produced from the interaction of the magnetic field and the metal in the microscope, since the magnetic field decays very rapidly. The sample stage was mounted externally so as not be coupled to the coils. The signal from the wave generator was passed through an amplifier before reaching the coils. A 300W amplifier (150W/channel) was enough to run sufficient current through more than 100 turns of wire. The field that was used throughout these experiments was 100 Oe. The signal from the amplifier was routed to an oscilloscope in order to get a precise measurement of the

frequency and the voltage at the output. Data acquisition was accomplished via a CCD camera that had been mounted on the microscope. The light microscope objective lens used throughout these experiments was 40X. The camera was connected to a computer for visualization and video capture. The video of the walkers was recorded on the computer and then transferred to a program that tracks their motion. The output from this program was distance vs. time data which was then imported into Mathematica for a more thorough and in-depth motion analysis. The entire apparatus can be seen below in Figure 7.

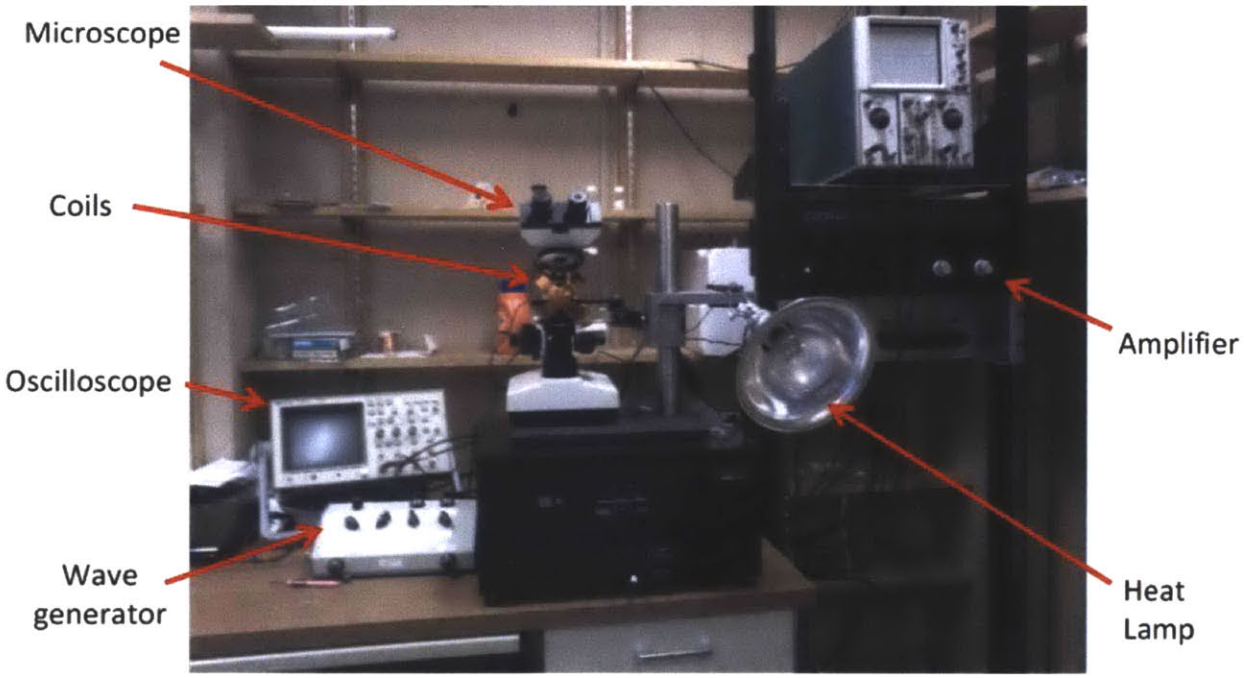

Figure 7: Visualization of "The Apparatus."

C. Investigating Superparamagnetism

During our experiments we noticed that a number of single bead walkers were exhibiting some finite, non-negligible, velocity. This didn't seem to fit with the description of the beads given to us by Solulink. If these beads were truly superparamagnetic, then single bead walkers shouldn't be able to walk. We hypothesized that these beads must not be completely

superparamagnetic but instead, have some finite paramagetism or coercivity. To investigate this phenomenon, we dropped 5μL of concentrated Soulink beads at a dilution of10mg/ml onto a biotin coated slide. The streptavidin coated beads were then stuck on the slide (due to biotin-streptavidin binding affinity) and placed in a VSM to measure a hysteresis loop. The VSM was ramped from -6000 Oe to 6000 Oe and the out of plane field was measured.

III. Results and Discussion

A. Walker Velocity Increases Linearly as Chain Length Increases

Following the protocol laid out in the above methods section, we set out to measure the velocities of walkers composed of 1, 2, 3, 4, and 6 beads. The frequency of the system was set at approximately 6Hz and the walker velocity was measured as the beads were walked across a 70μm track back and forth five times. The velocities were averaged and the standard deviation in velocity was captured in the error bars as seen in Figure 8.

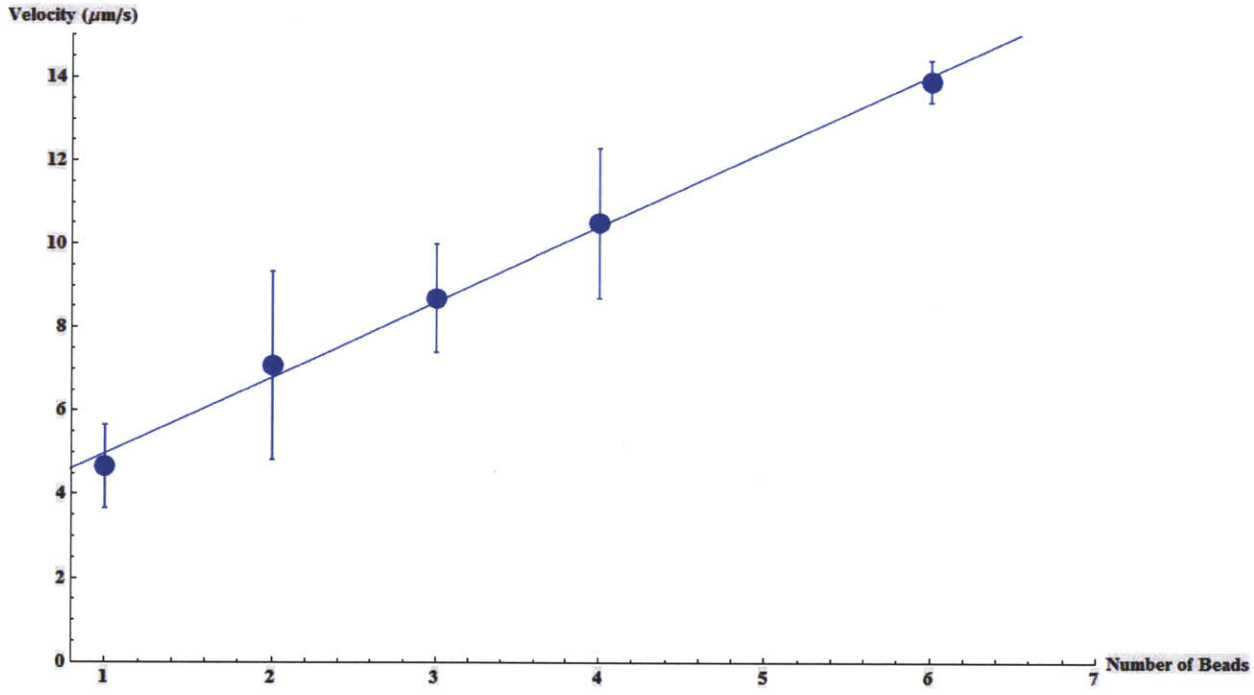

Figure 8: The velocity of the walkers increases linearly as the number of beads that composed the walkers increases.

The velocity of the walkers tended to increase linearly as the walker chain length increased with the addition of Soulink beads. This experimental trend matched with the previous theory on the motion of these walkers.[29] The velocity of the walkers was determined by the strength of the magnetic field being actuated, the length of the chain, the surface coefficient of friction, the viscosity of the fluid, and the frequency. In this experiment, the only variable that changed was the length of the chain which scaled linearly with the theoretical velocity

$$V_t = 2\nu l \tag{1}$$

where V_t is the theoretical velocity, ν is the frequency in Hz, and l is the length of the chain in μm.

B. Walker Velocity Increases Linearly as Hz Increases for Fixed Chain Lengths

For this experiment, a walker composed of two beads was isolated and the velocity was measured as the frequency was increased. The walker trekked back and forth across a 70μm track, back and forth five times at a particular frequency. The frequency was increased and the protocol was duplicated. The velocities were averaged and the standard deviation in velocity was captured in the error bars as seen in Figure 9.

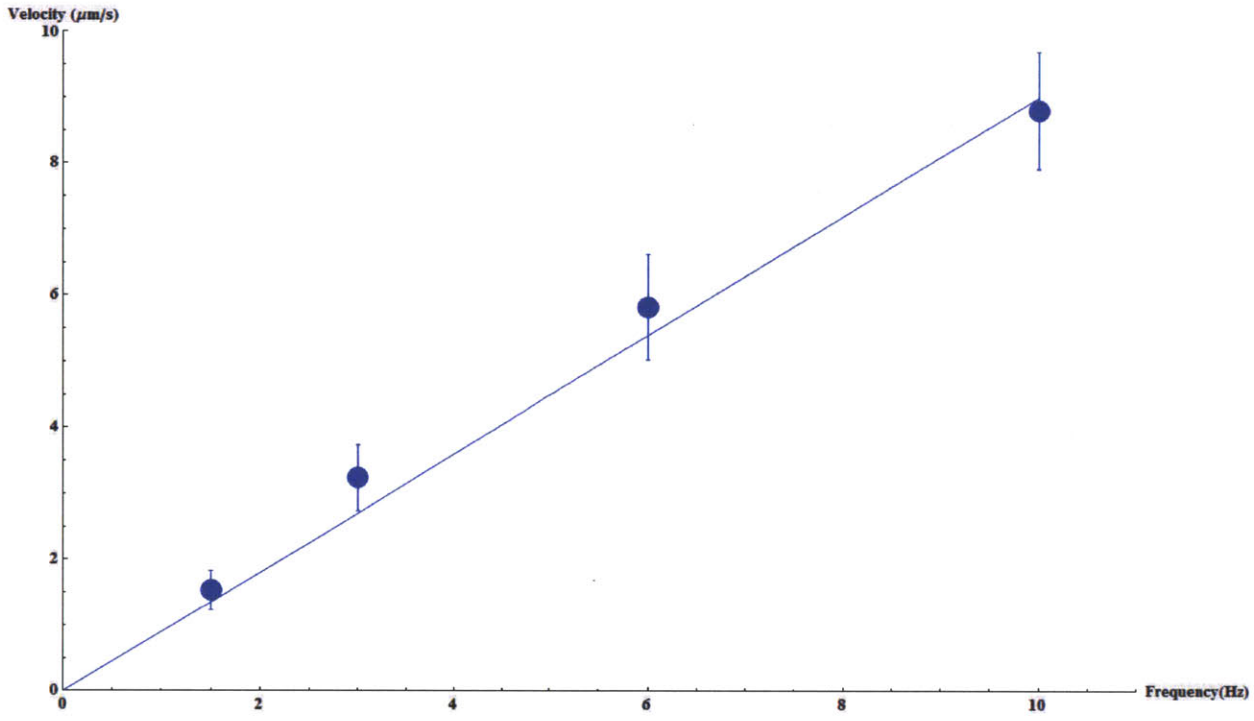

Figure 9: The walker velocity increases linearly as the frequency is increased.

Here, we again saw that the walker velocity increased linearly as the frequency was increased. This matches the already established theoretical constructs of this system as well as our equation for the theoretical walker velocity.

C. Solulink Beads Exhibit Some Finite Coercivity and Paramagnetism

From the previous experiments, we noticed that some of the "one bead" walkers had some distinct, non-negligible velocity. To insure this wasn't flow induced, we ran a number of experiments with extremely high dilutions on the range of 1:1000 beads per phosphate buffer solution. However, these one bead walkers still proceeded to move across the surface. If the Solulink beads were truly superparamagnetic, a single bead walker shouldn't have been able to move (see Figure 3). It's only when the beads self-assemble into larger chains that motion should be observed. The motion of these one bead walkers could be explained if the Solulink beads weren't completely superparamagnetic but instead exhibited some finite coercivity. The

hysteresis loop, seen in Figure10, was generated from a VSM, run at the specifications quoted in the previous methods section.

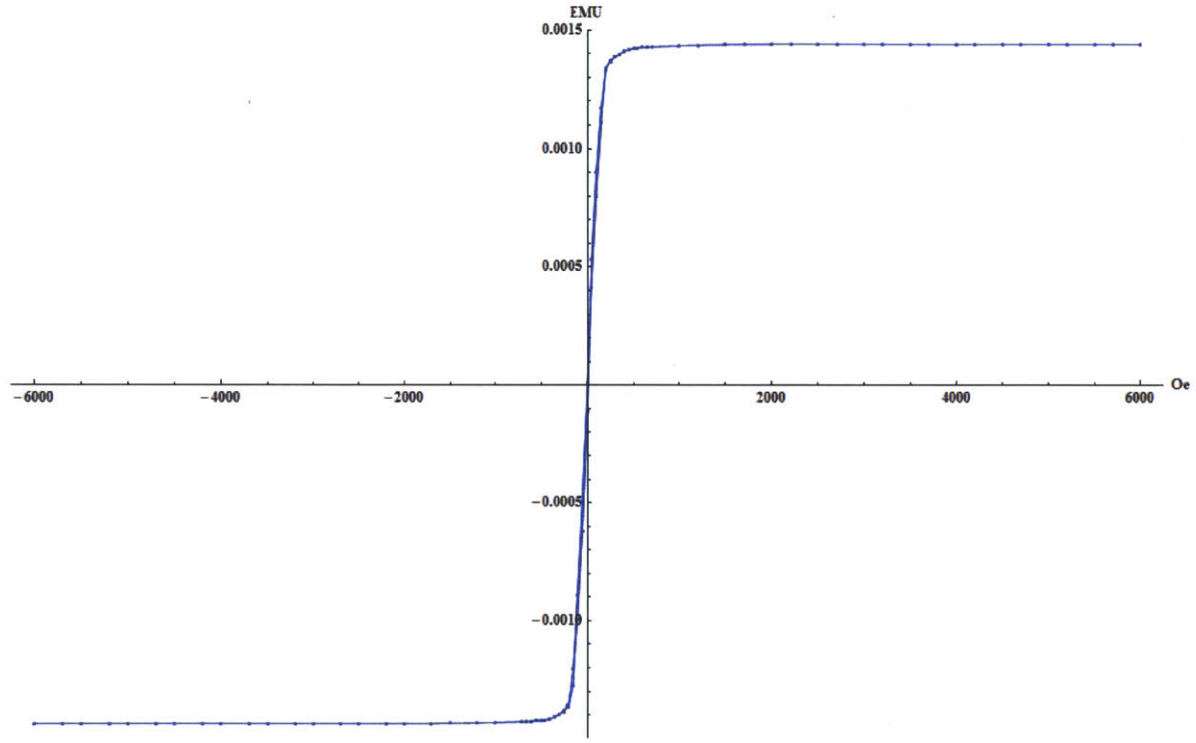

Figure 10: The Solulink bead hysteresis loop generated by a VSM. From this view, the beads appear to be superparamagnetic, explaining all of the previous walker behavior except the motion of one bead walkers.

The hysteresis loop appeared to be closed and the beads didn't appear to exhibit any discrete hysteresis. However, when we took a closer look towards the origin as seen in Figure 11, these beads actually exhibited some finite coercivity and a very small hysteresis loop.

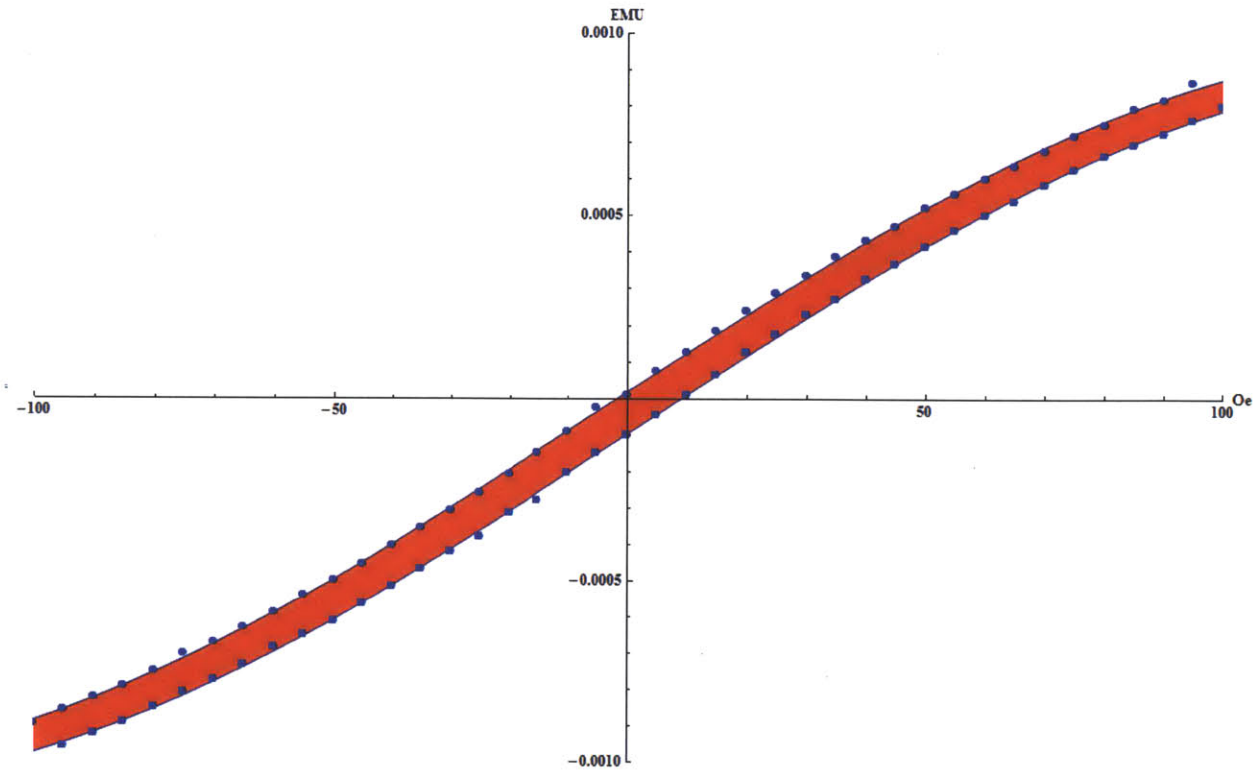

Figure 11: The Solulink beads actually exhibit a finite hysteresis loop, explaining the motion of the one bead walkers. However, this small coercivity illustrates that the beads are only very slightly paramagnetic so the superparamagnetic motion theory still holds and is experimentally observed.

This hysteresis loop explains the motion of the one bead walkers and the particularly small coercivity and hysteresis loop explains the very low velocity exhibited by these walkers. However, it should be noted that this also illustrated that these beads are only slightly paramagnetic, meaning that the previous superparamagnetic motion theory previously outlined still holds and was experimentally validated.

IV. Conclusion

Although our primary focus on this project was the creation of a chemotactic system, the above results are by no means trivial. The ability to characterize the motion of the walkers on an uncoated glass surface gives us the crucial baseline we require to accurately characterize and analyze our chemotactic system when the time came. We now have an accurate characterization

of walker motion, the knowledge that the glass slide doesn't induce any type of artificial velocity gradient, evidence of the paramagnetic behavior exhibited by the Solulink beads, and a cleaning protocol that enables efficient walker motion. Additionally, these results may have further implications in future offshoots from this project, particularly in controlling microfluidic motion at the nanoscale (see Chapter 5: Conclusions and Future Work).

Chapter 3: Creating a Chemotactic Environment

I. Introduction

A. Benefit of Ligand-Receptor Synthetic Chemotaxis Approach

In order to synthetically obtain chemotactic directed motion, we utilized the biological receptor-ligand pair of biotin and streptavidin. Manipulation of the biotin-streptavidin bond was ideal for this project due to its aforementioned high binding affinity. The exceptional binding adhesion exhibited by the biotin-streptavidin bond is due to its complexing structure where four biotin molecules fit snuggly within the pocket of one streptavidin molecule, as seen in Figure 12, and it takes approximately 160 pN to break this non-covalent bond. [40]

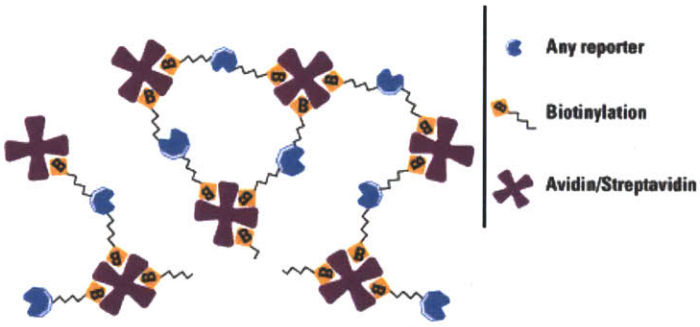

Figure 12 : Schematic of the biotin-streptavidin binding complex.[41]

These biotin binding sites provided the pivot or hinge point for the walkers. The subsequent increase in friction should lead to a larger velocity as opposed to the slipping that would occur in a region with a lower density of these binding sites, the manifestation of the idea outlined in Figure 3. It was therefore essential to tailor the coupling between the walkers and the surface (in both space and time), as it occurs in biological systems, to obtain optimal chemotactic directed motion. This was accomplished by creating gradients in the density of biotin receptors on the surface, the basic idea being schematically visualized in Figure 13.

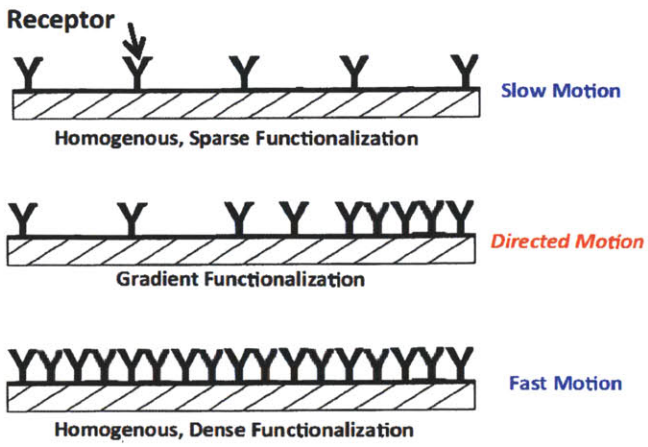

Figure 13: Lower velocities are due a lower density of receptor sites, leading to more slipping. Homogeneous areas with a higher density of receptor sites would provide increased friction and hinge points for walkers. Inhomogeneous gradient distributions are of interest for our purposes as they can provide the essential directed motion characteristic of chemotaxis.

B. Chemotactic System: Utilization of the Biotin-Streptavidin Bond and Solulink Bead Functionalization Using Biotin-PEG

The chemotactic system that we created utilized a biotin surface (via a biotinylated glass slide). Since the aforementioned walkers are coated with cross-linked streptavidin, in addition to creating a gradient in the density of binding sites a masking protocol had to be developed in order to reduce the biotin-streptavidin binding potential to allow for walker motion. But blocking all of the binding sites would simply result in walkers continually slipping with no significant translation. So the masking protocol must reduce the binding interaction potential but at least leave the minimal number of bonds required for some adhesion to the surface. The masking protocol that performed optimally in modifying the number and strength of the bonds is shown schematically in Figure 14.

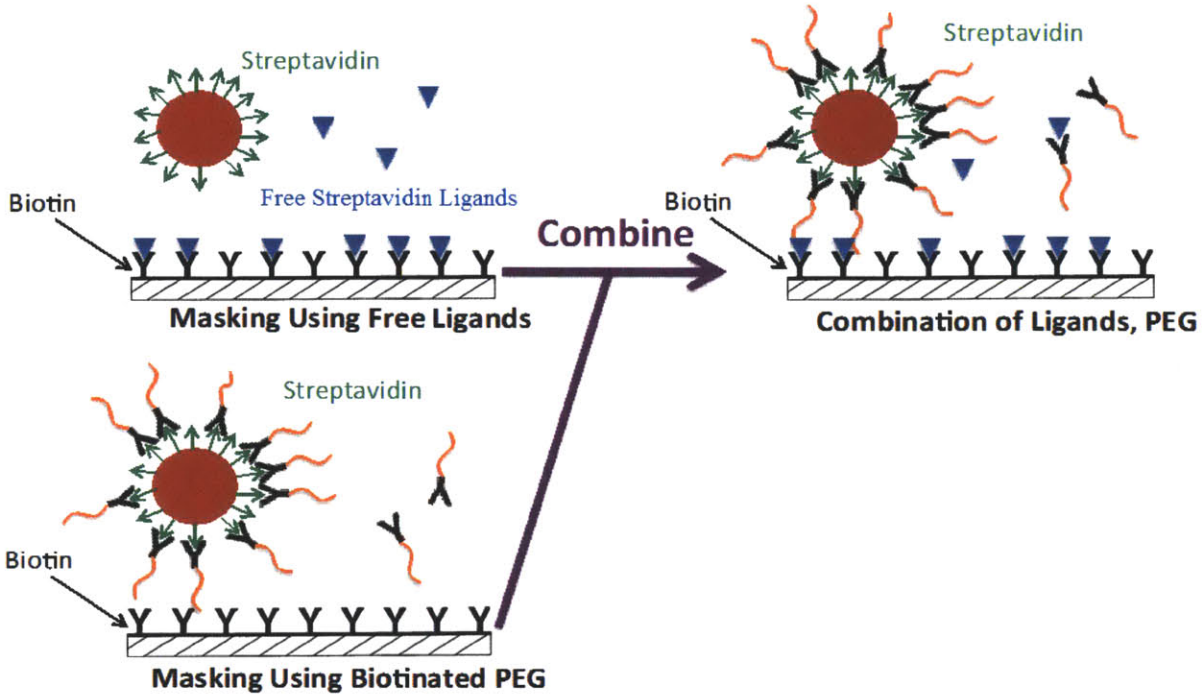

Figure 14: Schematic of the synthetic chemotactic system that utilizes the receptor ligand pair of biotin and streptavidin, in addition to the functionalized walkers coated with a biotin-PEG brush. This combination proved to be the optimal masking protocol

The first masking protocol utilized (upper left panel of Figure 14) aimed to cover the biotin binding sites with free streptavidin molecules. While in principle it is possible to cover all of the biotin sites with streptavidin and obtain walkers that continuously slip, our streptavidin concentrations were never high enough to completely coat the entire sample area. Although the walkers were able to move on this surface, the motion was marked by intermittent periods of walkers sticking to the surface (although by manipulating the frequency, they would eventually become unstuck) making velocity characterizations extremely difficult, if not impossible. To overcome this limitation, we combined the first protocol with a new protocol as seen in the lower left panel of Figure 14. The addition of this new protocol had two pronounced effects. It rendered the fraction of streptavidin binding sites (on the walker) that was engaged in binding to the biotinylated-PEG ineffective, thus reducing the number of available binding sites on the surface

of the beads. Additionally, this procedure changed the effective biotin-streptavidin binding interaction because in order for the streptavidin on the walkers to bind with the biotin surface molecules, the PEG brush had to be compressed. This would incur an entropic energy penalty since the compressed or collapsed state of PEG isn't a favorable entropic state. This increases the binding barrier and thus reduces the likelihood of the biotin-streptavidin binding. The new masking protocol prevented this intermittent sticking of the beads which allowed for continuous velocity measurements to be made. However, there were still enough free biotin binding sites on the surface (and streptavidin binding sites on the walkers) to allow for both hinge and slipping points. Additionally, even with the masking protocol the strength of the biotin-streptavidin bond was still strong enough to cause some sticking effect, a factor that became crucial for achieving chemotactic motion.

II. Methods

A. Droplet Method for Gradient Creation/Sample Preparation

To mimic a biological surface that was covered with biotin sites, we used biotinylated slides purchased from Xenopore. These biotinylated slides had biotin binding sites across the surface of the slide, each site 10nm apart (in the future slides with customizable patterns and surfaces can be provided by Microsurfaces Inc.). In order to make this homogeneous, dense functionalized surface inhomogeneous we had a number of different techniques at our disposal.[42-44] To create our gradients, a 50μL droplet of concentrated Streptavidin, 1mg/mL, was placed on the biotin slide in a 8mmx8mm area and allowed to evaporate overnight in a petri-dish. By letting the droplet evaporate and assuming a Gaussian evaporation pattern, we created a sufficient gradient in the density of biotin binding sites that would allow for directed motion. To get a rough

assurance that the biotin surface was binding to the streptavidin molecules, the contact angle of a water droplet was measured as a function of streptavidin exposure as seen in Figure 15.

Figure 15: Biotin is an extremely hydrophobic molecule with a water contact angle approaching 90 degrees. Streptavidin is highly hydrophilic with a water contact angle nearing 180 degrees. The water contact angle is increasing with exposure time of streptavidin, illustrating that the surface is indeed being coated with streptavidin.

Biotin is hydrophobic with a water contact angle approaching 90 degrees while streptavidin is hydrophilic, having a water contact angle nearing 180 degrees. The water contact angle measurement, seen in Figure 15, is approaching 90 degrees on the pure biotin surface with no streptavidin exposure, clearly illustrating the hydrophobic biotin surface. After exposure to streptavidin, the water contact angle begins to increase as the once purely hydrophobic surface is coated with hydrophilic streptavidin, illustrating that biotin-streptavidin binding is occurring. However, the length scale constraints of our experiments prevented gradient characterization purely by measuring water contact angle. Instead, gradients were measured by the velocity profile of the sample as well as via confocal microscopy (see Appendix: Gradient Quantification).

Before the concentrated streptavidin droplet was placed on the slide, the 8mmx8mm area was marked on the back of the biotin slide with a marker and the center of the square was also marked. This point not only marked where the droplet should be placed, but also marked the

sample origin. After the droplet was dried, the droplet residue was wiped off (see Appendix: Dendritic Formation) with a Kimwipe soaked in water and then dried with another Kimwipe. A channel was created around the droplet using the previous procedure utilized for channel creation. The glass coverslip was also cleaned using the same procedure.

Prior to channel creation, a 1:50 bead to aqueous solution was mixed at a 1:1 ratio with biotin-PEG (Nanocs Inc. 5000g/mol) at a 100mg/mL dilution. This solution was placed into a separate plastic cuvette and left to incubate at room temperature for at least twenty minutes. After the incubation period the solution was further diluted in an aqueous solution at a 1:100 ratio of biotin-PEG functionalized beads to water. Then 40-50μLs were inserted into the channel before the sample was placed on the sample stage in the apparatus.

B. Velocity Measurement Protocol

We developed a systematic method in order to generate a velocity profile of the sample. The frequency for this set of experiments was set at 1Hz. We sought to characterize the velocity of the sample from approximately -300μm to 1000μm along the x-axis of the sample using the droplet guiding dot as the origin. Only two bead walkers were analyzed for the remainder of the experiment primarily because they were by far the most prevalent in the sample and because their rotor-like motion was far superior to any other chain length walker. The 40X objective gave us a 150μmx150μm area to characterize velocity. A walker was isolated and placed at the edge of the screen. The field was turned on and the walker velocity was characterized for a 100μm long track. The walker ran across this track back and forth five times. The walker was then moved to the other edge of the screen and made to walk across another 100μm track, towards the old starting point this time. The walker ran across this track, back and forth five times once again, giving us an overlapping area of velocity of approximately 50μm. After the final run, the

screen was moved 150μm and the process repeated across the aforementioned area of interest. The five runs moving left and right were averaged and that value was given as the velocity in the center of the area it was traversing. For example, if the walker was walking from 0-100μm in the sample, the average velocity would be plotted at the 50μm mark in the sample distance. The standard deviation in velocity was captured in the error bars in the velocity profile graph. The velocity profile is actually the normalized velocity across the sample with the normalized velocity being the velocity at the very edge of the sample, which is completely coated in streptavidin and approximately matches the velocity on the uncoated glass surface. Additionally, the blue plot markers denote velocity when the walkers moved forward (position is increasing with respect to the sample region) while red marks denote velocity when the walkers moved backward.

C. PEG Binding Calibration

Another crucial parameter for these experiments was calibrating the optimal biotin-PEG coverage of the streptavidin coated bead for our masking protocol. We determined that the proper biotin-PEG coverage would be one that optimized the velocity of biotin-PEG functionalized beads on a biotinylated surface. The same slide cleaning and channel creating protocol was followed from previous experiments as well as the method to create biotin-PEG functionalized walker solutions. Several channels were created on the pure biotin glass slides and the velocity of biotin-PEG functionalized walkers was analyzed for incubation periods of 0min, 5min, 10min, 20min, 30min, and 40min, all at room temperature. Only two bead walkers were isolated and the velocity at 2Hz was analyzed. They were made to walk across a 70μm long track, back and forth five times. The velocity was analyzed and averaged for the five runs; the standard deviation in the velocity was captured in the error bars.

III. Results and Discussion

A. Biotin-PEG Binding Saturation Of Solulink Beads Occurs After Incubation Period of 20 Minutes at 25°C

When running the experiments to calibrate the optimal biotin-PEG coverage of the Solulink beads, the initial velocity measurements taken at 0, 5, and 10 minutes of biotin-PEG incubation exhibited some strange behavior. Walker motion was punctuated by extended periods of sticking and beads would occasionally "jump" or rather "hinge" somewhat violently in the course of their trek. This led to velocity measurements that exhibited a high degree of variability as seen in the error bars in Figure 16.

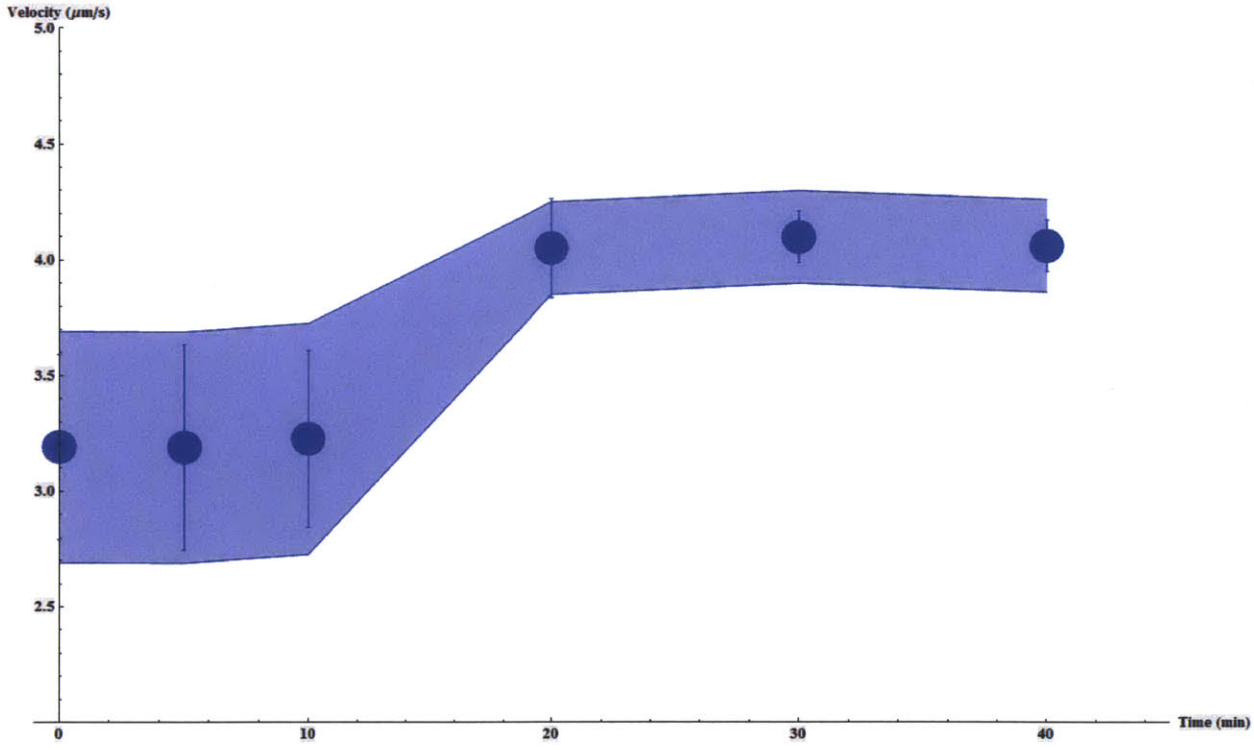

Figure 16: Biotin-PEG calibration for optimal coverage of the Soulink beads to be utilized in the masking protocol and used in all subsequent experiments. The velocity was significantly lower and exhibited more variability. The walker motion at this time was also somewhat erratic, punctuated with periods of sticking. Twenty minutes appears to be the optimal incubation time to get complete coverage. A longer incubation period does very little to walker motion as the biotin-PEG coverage is completely saturated.

The kinetics of the biotin-streptavidin bond most likely didn't allow for complete biotin-PEG coverage which caused the walkers to be more exposed to the environment, causing the sticking. Additionally, the incomplete coverage could have caused the PEG to undergo some type of phase separation (see Appendix: Effect of Temperature and Salt Concentration on PEG Phase Separation) which would also explain this strange walker motion. However, when analyzing the motion of the walkers after an incubation period of twenty minutes there were virtually no instances of sticking and the walker motion markedly improved. Interestingly, this led to an increase in the velocity but this can probably be attributed to a return to a more "normal" type of walker motion. Further velocity analysis at longer incubation periods, even at incubations periods exceeding several hours (not shown in Figure 16), were consistent with the motion observed for walkers incubated for twenty minutes. It appears that after an incubation period of approximately twenty minutes, the biotin-PEG coverage becomes saturated. This is the incubation period that was utilized for all subsequent experiments that utilized this type of masking protocol.

B. Velocity Profile of Sample Illustrates High and Low Density Areas of Biotin Binding Sites

The velocity profile of our sample region of interest, approximately -300μm to 1000μm, can be seen in Figure 17.

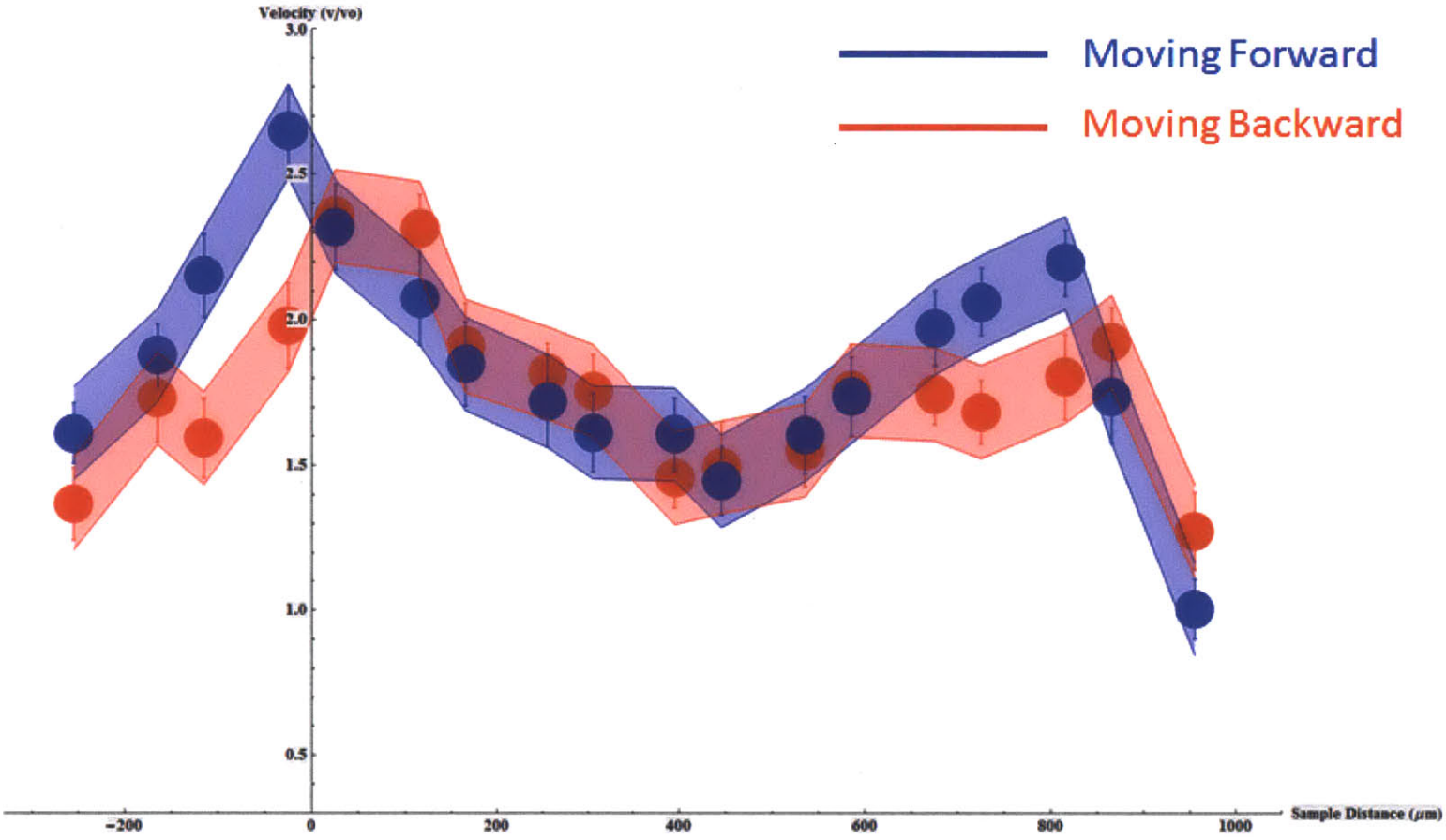

Figure 17: Velocity profile of the sample region of interest. There are two clear peaks in velocity at approximately 0μm and 800μm as well as a relative minimum at 450μm. There are also several velocity transitions that could be evidence of chemotactic directed motion as the velocity going toward an area with a high density of binding sites is markedly greater than the velocity away from those sites.

The most prominent features present in this velocity profile were the two peaks in velocity located at approximately 0 and 800μm as well as the local minimum in velocity at approximately 450μm. From our previous theoretical construct concerning walker motion (specifically how the presence of binding sites permit hinge-like motion and an increase in friction while covered sites cause the walkers to slip), it clearly appears that in our sample region of interest we have two regions with a high density of binding sites as well as a region that has a lower density of binding sites. These regions with a high and low density of binding sites are crucial in creating the chemotactic system as the walkers should tend to drift toward the regions with a high density of binding sites due this almost twofold discrepancy in normalized velocity. Perhaps a more subtle

and interesting aspect of this velocity profile are the different transitions or more appropriately, regimes where one walker direction of motion exhibits the "dominant" velocity. From our starting point of approximately -300μm, walkers moving forward exhibited a marked increase in velocity over their backward moving counterparts. At approximately 0μm, we saw the dominant direction of motion change so that now the backward moving counterparts exhibited a slight but appreciable velocity difference. The dominant direction changed at approximately 450μm and once more at 800μm. Even for these continuous velocity measurements, we were beginning to see evidence of the chemotactic system we created. In each regime we outlined, the velocity moving towards an area with a high density of binding site was larger than when the walkers were moving away from that area. Thus it appears that even infinitesimally small changes in biotin binding density can have a pronounced effect on walker motion.

IV. Conclusion

In our continuing attempt to create a chemotactic system, we first had to create a chemotactic environment which was accomplished by creating a gradient in the density of binding sites by placing a droplet of concentrated streptavidin on our biotin-coated slide surface and letting it evaporate. The droplet proceeded to evaporate in a Gaussian manner, producing wave-like gradients in the density of binding sites. Additionally, we developed a masking protocol to optimize the motion of the walkers without completely eliminating the binding interaction potential of the biotin-streptavidin pair and thus the chance to mimic chemotaxis. In the development of this masking protocol, it was determined that the appropriate incubation period to obtain the optimal coverage of biotin-PEG on the walkers was twenty minutes at 25°C. Finally, the discrepancy in velocities exhibited by the velocity profile of the sample region of interest illustrated two regions with a high density of binding sites, at 0μm and 800μm, as well as

a region that exhibited a local minimum in density of binding sites at 450μm. Additionally, some evidence of chemotactic directed motion was beginning to be observed as the velocity of walkers traveling towards regions with a high density of binding sites was much higher than the velocity of walkers moving away from these regions.

Chapter 4: Breaking Symmetry: Further Evidence of a Chemotactic System

I. Introduction

A. A Closer Look At Chemotactic Movement Dynamics: Chemotactic Drift

The velocity profile illustrated that our method of gradient creation was successful in creating regions with a high and low density of binding sites. Furthermore, our initial hypothesis of modulating the walker velocity by increasing or decreasing the density of binding sites was proved correct. When the walkers were in regions with a high density of binding sites; their velocity noticeably increased. This was due to the increased friction provided by these binding sites, allowing for hinge-like motion. Meanwhile, walker velocity dropped when they were in regions with a low density of binding sites. This decreased effective friction resulted in walker motion marked by an increase in slipping. However, this is not yet evidence of chemotaxis. Chemotaxis is directed motion toward or away from the direction of a chemical gradient. In order to synthetically create a chemotactic system, we must be able to observe net motion toward regions with a high density of binding sites.

If we have truly created a chemotactic system, we should be able to observe this net motion even when the walkers are actuated in a completely random manner. If even the simplest random protocol were utilized to drive walker motion in random directions, this inherent velocity discrepancy in our system would cause the walkers to drift toward areas with a high density of binding sites. By implementing this random protocol, we would remove any bias and should be able to see these walkers drift towards the gradient. We would then be able to extract this drift force or drift velocity, in addition to achieving the first instance of synthetic vectorial chemotaxis.

II. Methods

A. Intensive Motion Analysis Across Gradient

In order to get a better idea how these walkers moved in this chemotactic system, we developed a new protocol that allowed us to analyze "discrete" walker motion across the sample. The frequency used was once again 1Hz and the sample preparation protocol that was developed to generate the previous "continuous" velocity profile was utilized for this set of experiments. Furthermore, the "screen-moving" protocol that was previously used was duplicated here. The only distinction being that instead of measuring the "continuous" walker velocity profile across the sample, here we measured the "discrete" walker velocity profile across the sample. By "discrete" we mean that the field was actuated for approximately three seconds, then turned off for a duration ranging from two to three seconds, and then turned on again for approximately three seconds. This process was repeated until the walker moved across the 100μm track and back three times. The walker was then moved to the next track and this process was repeated across the sample. Each "discrete" walk was then analyzed in Mathematica, specifically calculating the time the walker spent moving and the distance it traveled. Each discrete walk across the track was analyzed, averaged, and plotted in the same way as the continuous velocity profile.

B. Applying a Random Walk/Monte Carlo Method to Investigate Chemotactic Motion

In order to observe chemotactic drift, the following random walk/Monte Carlo protocol was developed. We wrote a simple program in Mathematica that randomly generated a number between 0 and 1. If the number was larger or equal to 0.5 the field would be rotated forward, causing the beads to move forward and if the number was less than 0.5, vice versa. This protocol required that we retain the number of rotations per "coin-toss" to be constant. However, since we

were operating at a constant 1Hz we simply fixed the duration of the walk set at approximately two seconds, which translates to actuating in any given direction for the same amount of time.

To investigate our chemotactic system, a "short" series of random walk tests were conducted, using the previous protocol outlined above, with walker starting positions chosen (in a pseudo-random manner) to be 30μm, 760μm, and 300μm in reference to the sample distance. For each two bead walker at each position, 100 "coins" were flipped. The distance traveled during each discrete walk was analyzed and a table of positions on the sample was generated. Since the walker doesn't move when the field isn't actuated, it was relatively simply to convert this distance data into position data with the starting point as a reference. Approximately 300 position points were used to construct a histogram which we expected to illustrate chemotactic movement to areas with a high density of binding sites. After this "short" series of tests, a more comprehensive series of "long" random walks was run. In this protocol, the starting position of the two bead walkers was determined to be 0, 40, -30, 400, 350, 300, 550, 600, 635, 770, 800, and 840μm on the sample. At each position, 300 "coins" were flipped and a histogram was constructed in the same manner for the "short" series of tests.

C. "Back-and-Forth" Protocol to Derive Drift Force/Velocity

In principle, it is possible to extract some type of drift term by analyzing the data collected in the experiment above. However, in order to extract the "true" drift velocity or force term we must remove any bias that the "coin" toss protocol could inadvertently produce. Thus, we developed a new "back-and-forth" protocol in order to extract this drift term. Once again, only two bead walkers were observed with the frequency set to 1Hz. This time beads were strategically placed according to the "continuous" velocity map previously developed. Beads were placed near the bottom of the velocity hill, approximately 450μm. This was done so we

could observe whether this system was truly chemotactic by pushing the system to the limit and seeing if the beads would "sniff" out the area with a high density of binding sites, thus exhibiting chemotactic drift. Beads were placed at either end of this local velocity minimum, about 300 and 600μm respectively. These positions placed the walkers at a position where binding density and thus, velocity was very low but still within the "rip current" of the chemotactic system where we could observe some vectorial chemotactic motion. The field was then actuated forward for two seconds, and then turned off for approximately two to three seconds, and then actuated backward for two seconds and turned off again. This protocol was repeated for approximately 300 "steps" or until the walkers reached the top of the velocity peak and proceeded to get "sucked" into this region and no longer exhibited any drift. The position data was collected in the same manner as in the section previously described and then plotted against the amount of time the bead was traveling. The drift velocity was extracted from this plot using a simple linear fit to the data.

III. Results and Discussion

A. Symmetry is Broken By Time Lag at Areas with a High Density of Biotin Binding Sites

To obtain chemotactic motion, the symmetry of the system had to be broken. This was accomplished by the binding density discrepancy which lead to the velocity discrepancies and thus, an optimal path. The results of our comprehensive discrete motion analysis, seen in Figures 18 and 19, illustrate how symmetry was broken in the system and how chemotactic motion was accomplished.

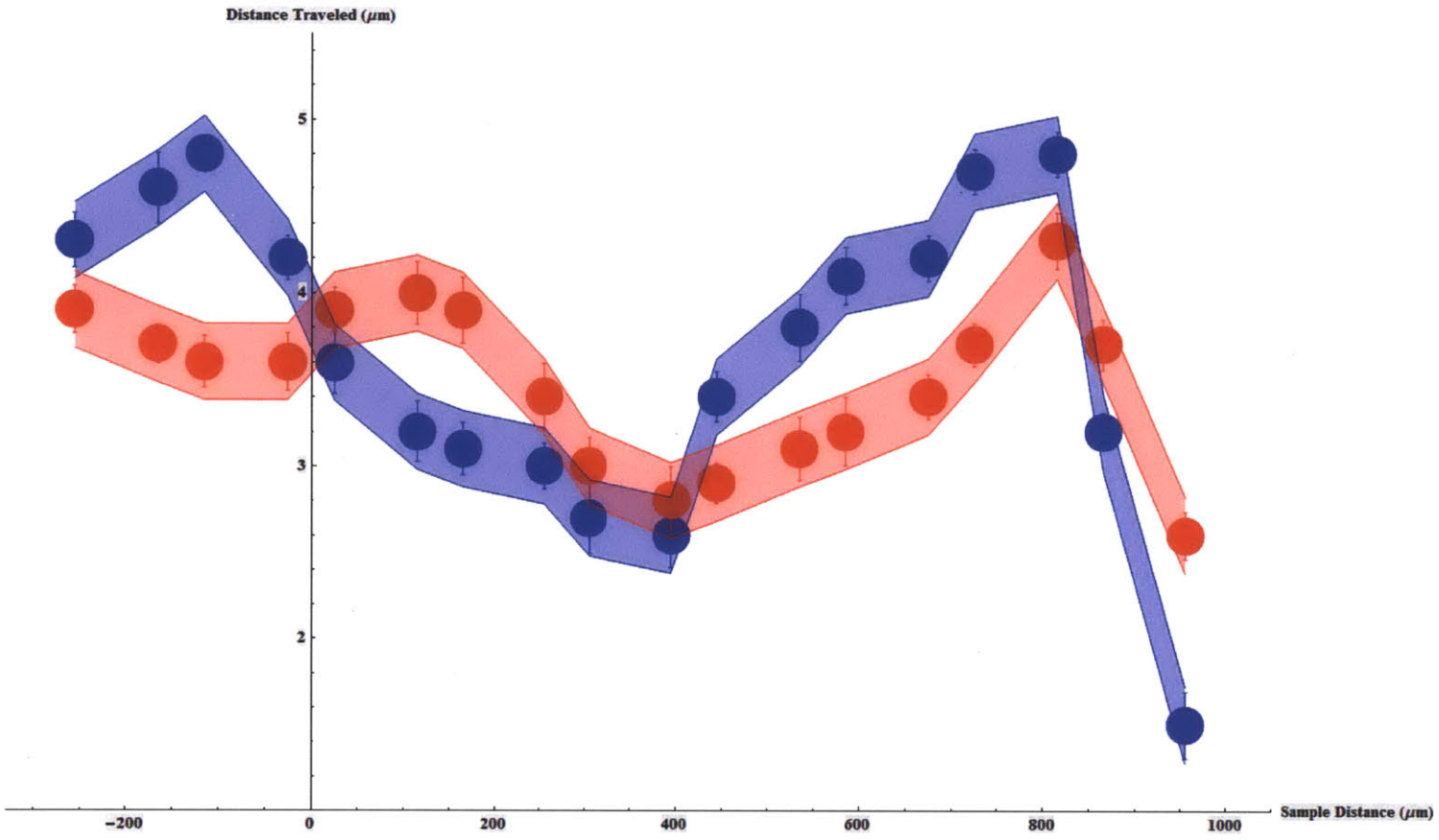

Figure 17: The average distance traveled for the discrete set of experiments is plotted across the sample region. Here we can really see evidence of chemotactic directed motion as the distance traveled is always greater for walkers moving toward regions with a high density of binding sites. The beads are drifting or being pulled towards these regions. (Note: the color denotation for the continuous measurements remains the same for the next series of graphs)

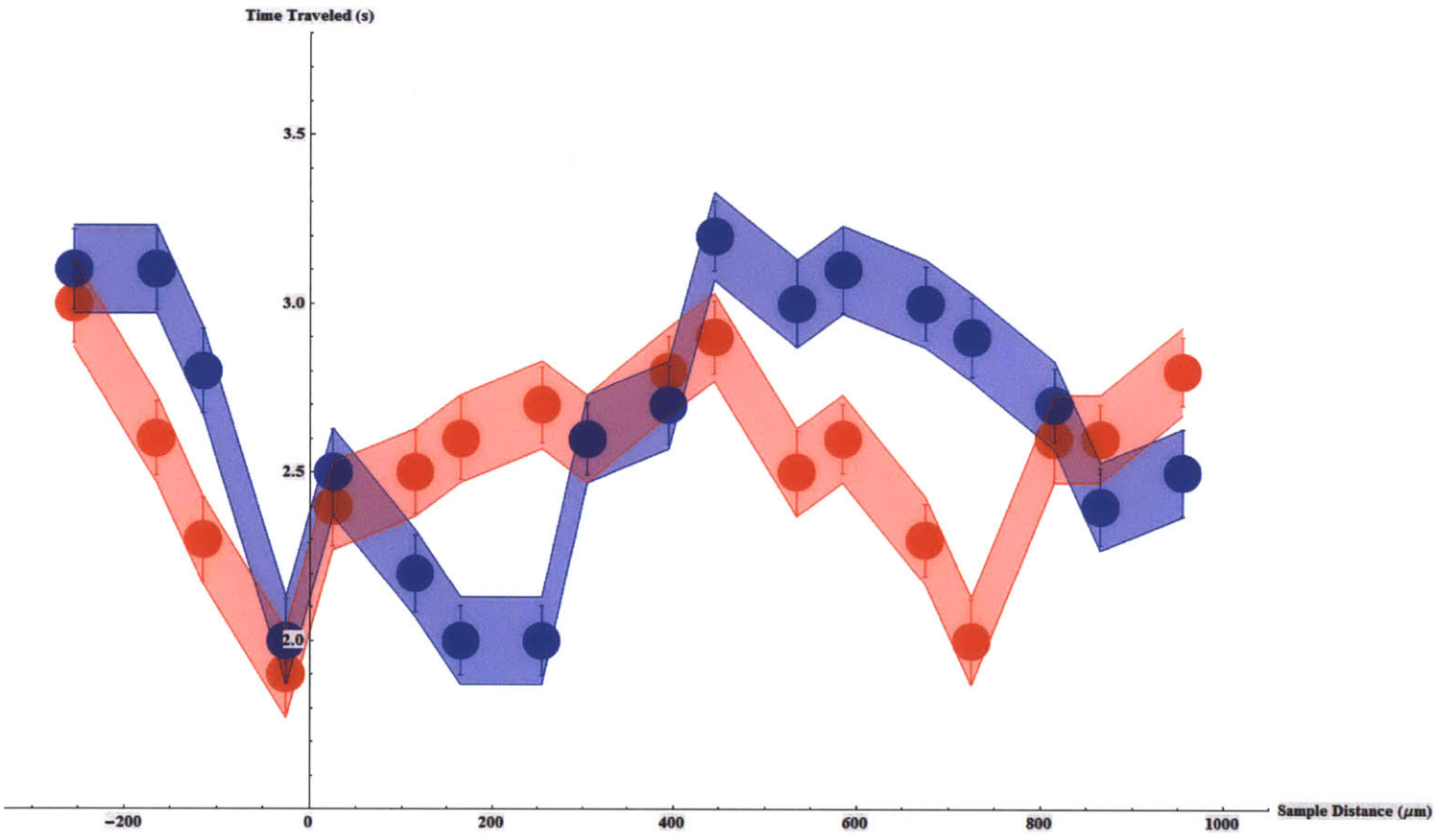

Figure 18: The time the walkers traveled across the sample region is plotted here. We see a marked dip in the time traveled at regions near 0μm and 800μm. These regions have a high density of binding sites which caused the walkers to stick for a portion of their approximate 3 second walk. Meanwhile, the longest walking time occurs near 450μm because this area has an extremely low density of binding sites.

There was clearly a marked decrease in the time the walker traveled for walkers near 0μm and 800μm. Under completely ideal conditions these walkers should have travel for approximately three seconds. Meanwhile, walkers that were near 450μm walked for the entire time the magnetic field was actuated. This behavior was directly linked to the density of binding sites. The walkers that were near 0μm and 800μm were in an area that had a high density of binding sites. As a result, these walkers tended to stick when the magnetic field was initially actuated. They would eventually start to wiggle, and then released, experiencing no more sticking for the rest of the walking period. Referring back to Figure 18, we see that once these beads started moving, they clearly exhibited this hinge type motion previously theorized. Walkers that were near 450μm on

the other hand were in an area with a low density of binding sites. As a result, they could "lift" off from the surface quite easily when the field was actuated because the binding interaction potential of biotin-streptavidin was significantly lower than the 0 or 800μm regions. However, the actual translation of these beads was quite small considering they were moving for approximately three seconds. Here the beads didn't exhibit hinge-like motion but instead slipped, due to the low density of binding sites or hinge points which significantly reduced translation. These were the motion mechanics which broke the symmetry of this system. The density of binding sites leads to either "hinge-or-slip" motion, which leads to a velocity discrepancy and gives rise to chemotactic or directed motion towards areas with a high density of binding sites.

B. Beads Exhibit Chemotactic Directed Motion via Aggregation at Areas with a High Density of Biotin Binding Sites

We have seen that chemotactic motion is possible as the discrete velocity measurements illustrated how the symmetry of the system is broken. Yet, in order to definitively illustrate chemotaxis, walkers should drift toward these regions with a high density of binding sites regardless of the direction of motion or "path" they take. Thus, when we place these walkers on a random walk path they should drift toward areas with a high density of binding sites; which in our sample is at approximately 0 and 800μm. This drift towards areas with a high density of binding sites is illustrated by the histogram in Figure 20.

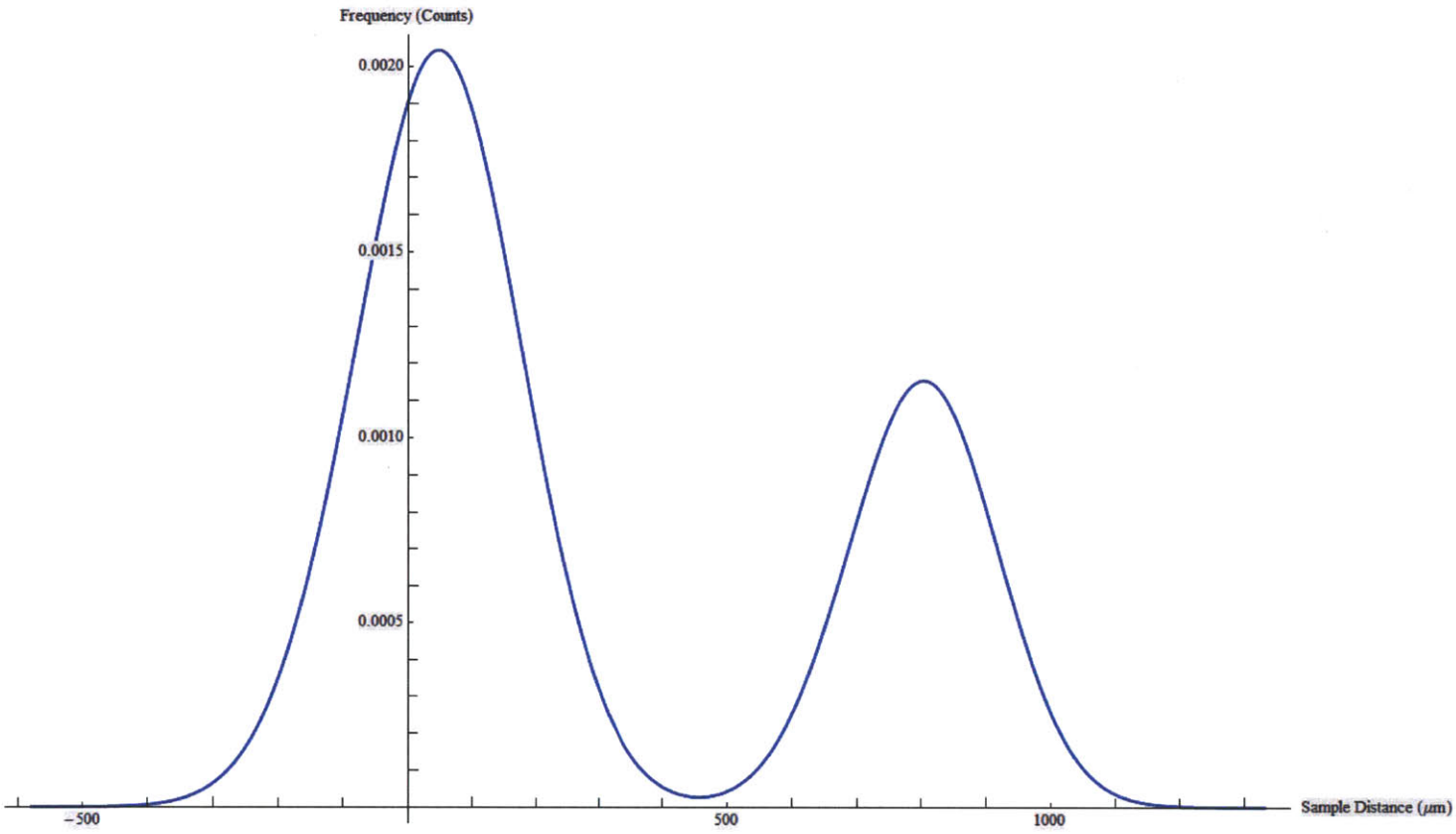

Figure 20: As the histogram indicates, even from this very short random walk experiment we see aggregation of walkers into the two regions with the highest density of binding sites. The beads are able to sniff out these regions and then are pulled into them, achieving chemotactic motion.

This histogram was generated using the "short" random walk protocol previously described, but even the walkers set on this short random walk path exhibited a strong chemotactic drift towards areas with a high density of binding sites. The drift was also clearly observed during the experiment, particularly the hinge-like motion when moving towards a high density area and slipping motion when moving towards a low density area. Furthermore, once the walkers drifted into an area with a high density of binding sites, they tended to stay in that area for the duration of their random walk path. Actually, it was virtually impossible for the walker to leave the area on its random walk path; the only definite way for the walker to leave an area was if it was taken off of its random walk path. Interestingly, if the walkers were placed in an area with a low density of binding, for example near 450μm, the walkers didn't seem to stay stuck in these areas

in a similar manner as if they were at 0 or 800μm. The random walk fluctuations seemed to be enough to move the walkers a sufficient distance to get out of this local minimum and get caught in the "drift current." Once in this current, the walkers continued to drift towards an area with a high density of binding sites seemingly regardless of the random walk path they took. The reason for this behavior was most likely due to the inheterogeneous nature of the gradient creation. The presence of several unbound sites was enough to allow the walkers to translate enough and enter the drift current. However, in an area with a high density of unbound sites, the presence of several bound sites wasn't enough to eliminate the hinge-like motion and the resulting chemotactic pull. Even if these covered sites slightly reduced the hinge-like motion of the walkers, once the walkers continued their random walk path, the sheer number of unbound sites in these areas drew the walkers back into these regimes once more.

In order to make sure the results in Figure 20 weren't due to the conditions of the "short" random walk protocol, we expanded this protocol in the "long" random walk protocol which vastly increased the number of coin flips per random walk and increased the number of walker starting points. The resulting histogram can be seen in Figure 21.

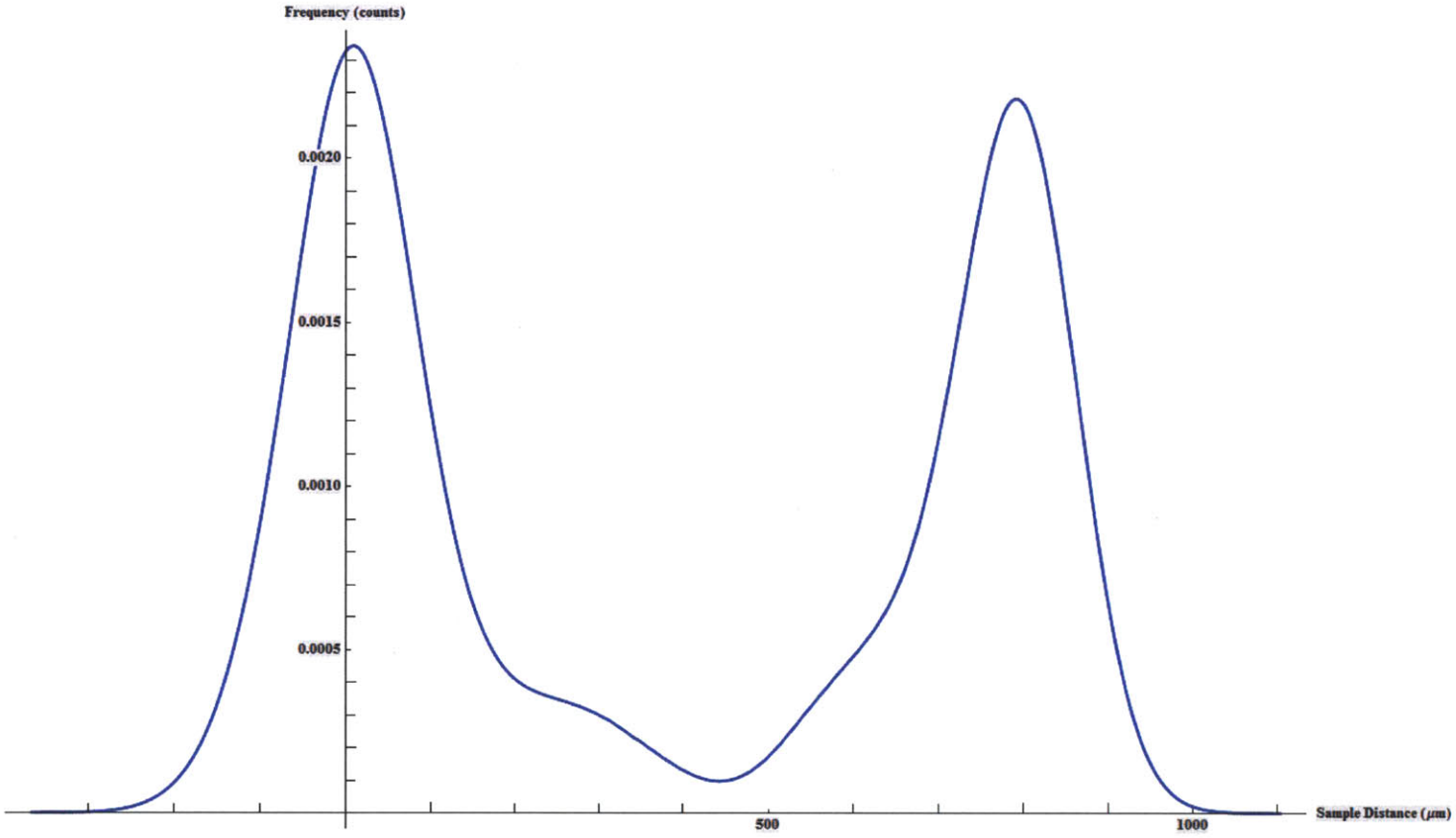

Figure 21: Even when the walkers are started at a variety of different locations and are given more coin tosses, we still see that these walkers aggregate into these two regions. This is truly a chemotactic system.

Clearly, the previous analysis still holds true for this new protocol. Even when these walkers were placed on an extremely long random walk, giving them ample opportunity to occupy previously inaccessible states or to even leave areas with a high density of binding sites, they continued to drift towards and stay in areas with a high density of binding sites. We have succeeded in synthetically creating the first chemotactic system with walkers that exhibit chemotactic drift.

C. Two Distinct Drift Velocities Illustrate Chemotaxis and Differences in Density of Biotin Binding Sites

We have experimentally observed chemotactic drift by placing the walkers on a random walk and witnessed walkers drifting toward areas with a high density of binding sites. However, we

can further characterize this system by extracting a drift velocity from the walker position data. We could do this from the data we already have from the random walk paths however, this would not be the true drift velocity. No matter how random we think our coin flip program to be, it may spit out coin flips that are biased toward a particular direction of motion. In order to eliminate any statistical bias in the drift velocity term, we must simply actuate the walkers backwards and forwards to see if they drift towards an area with a high density of binding sites. This was first done for walkers placed in the "drift current" that took them to the 0μm area as seen in Figure 22.

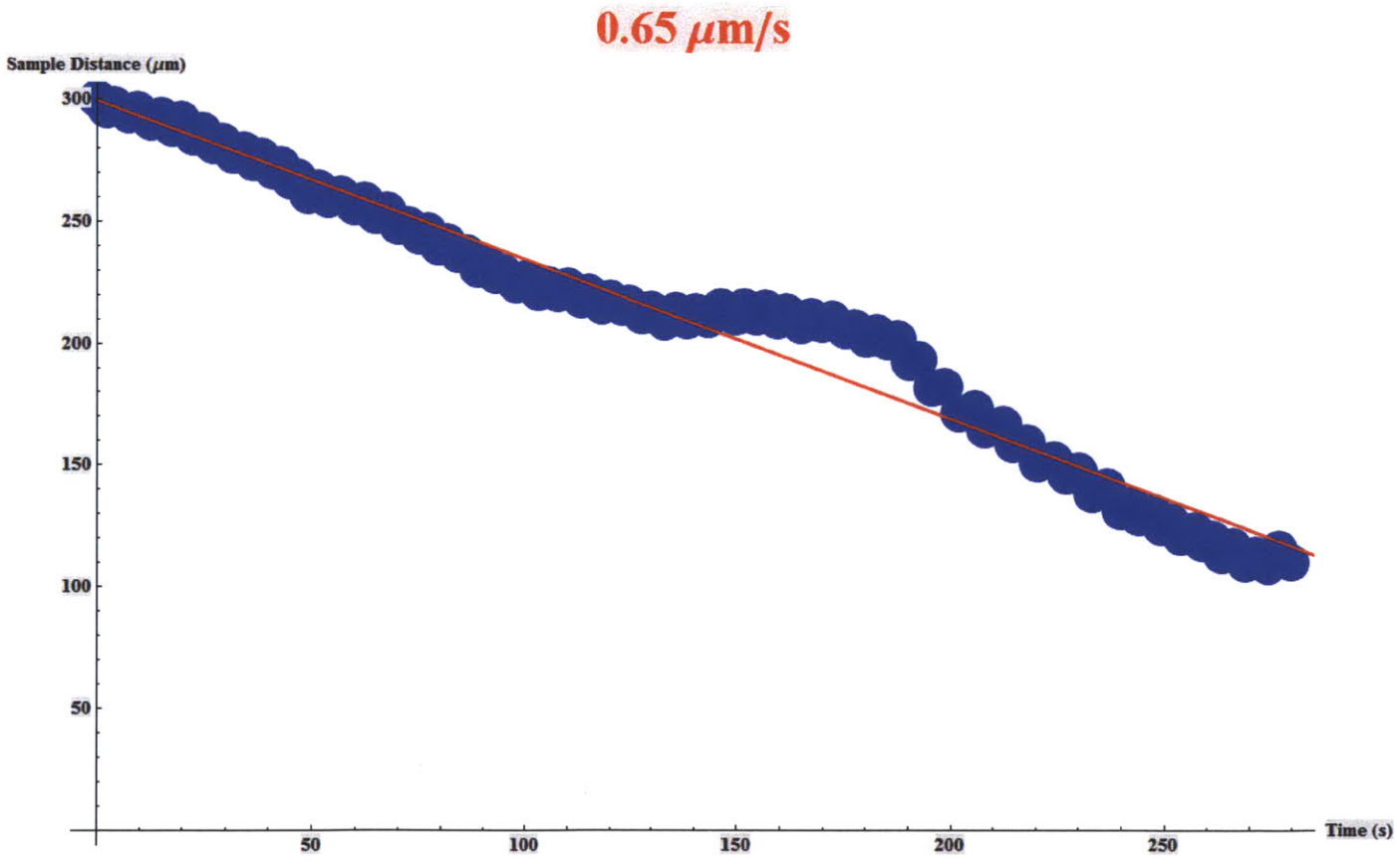

Figure 22: Here we can actually see how the walkers drift towards regions with a high density of binding sites as the actual position of the walkers is plotted against the total time of the discrete walks. We observe a linear trend and find that the drift velocity for beads drifting towards the 0μm region to be approximately 0.65μm/s.

The position of the walker during this "back-and-forth" protocol is shown plotted against the time the walker moved. We can clearly see drift occurring and the drift appears to be roughly

linear. The drift velocity was found to be approximately 0.65μm/s. Interestingly this was noticeably larger than the drift velocity calculated for walkers placed near the "drift current" that takes them to the 800μm area as seen in Figure 23.

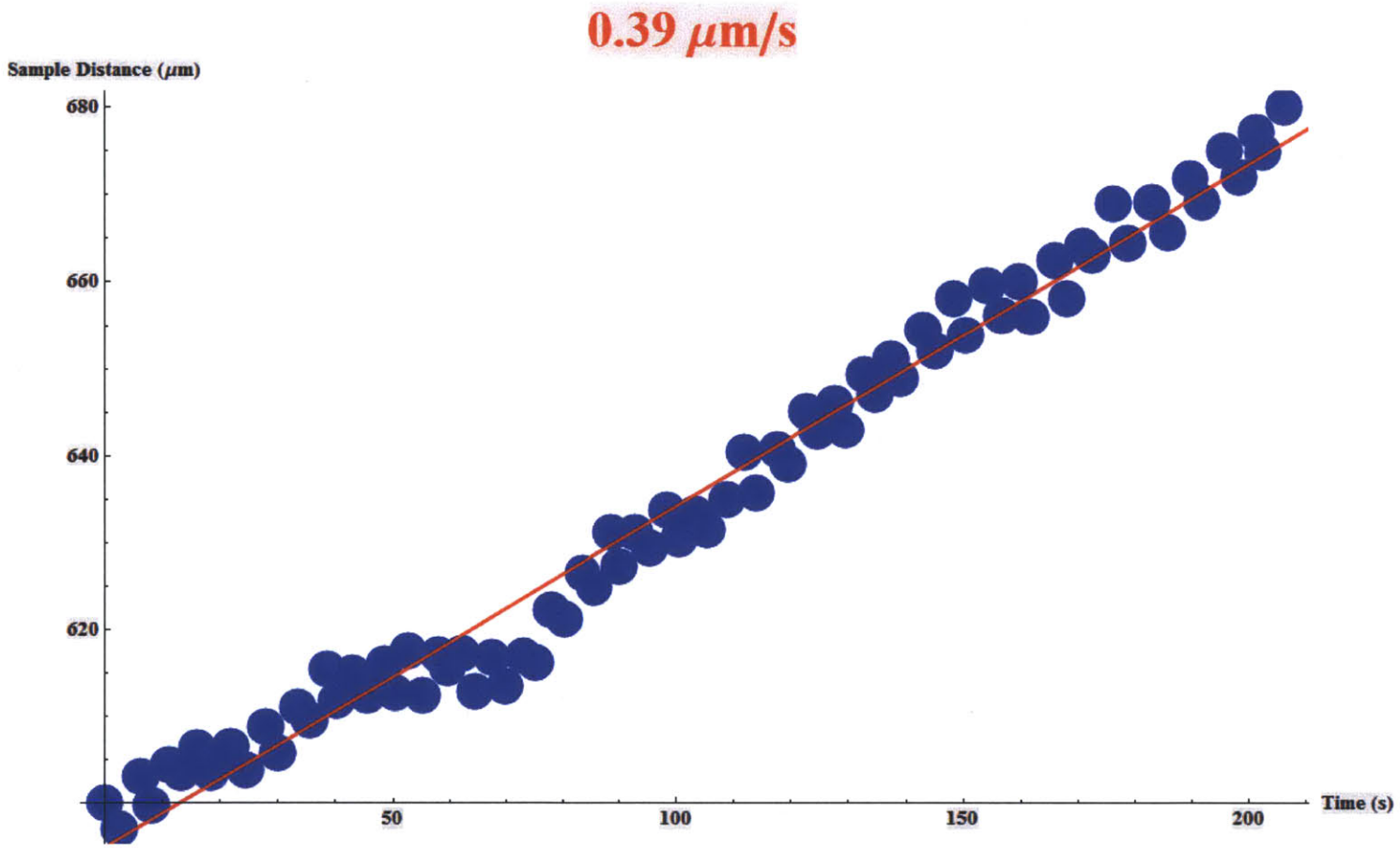

Figure 23: We again see this linear trend but for walkers drifting towards the 800μm region is only 0.39μm/s, noticeably lower than the drift velocity of walkers drifting toward the 0μm region. This is to be expected since the velocity profile of the sample clearly indicates that the 0μm region has a high density of binding sites since this region exhibited the maximum velocity. Therefore, the gradient in the direction of the 800μm is smaller than the gradient for the 0μm direction.

Here, the drift velocity was found to be approximately 0.39μm/s. This should be expected from the continuous velocity profile seen in Figure 17. The 0μm area had a slightly higher velocity than the 800μm area, signifying that the 0μm region had a higher density of binding sites and therefore, a larger gradient. The drift velocity should be directly proportional to the gradient so this finding was consistent with our velocity profile.

IV. Conclusion

By conducting a series of discrete velocity runs, we were able to analyze the motion of the walkers in the chemotactic and actually observed where the symmetry in the system was broken. Our analysis was consistent with our initial theoretical framework as the walkers experienced a significant amount of "sticking" followed by hinge-like motion when the walkers were present in a high density area. When the walkers were in a low density area, they exhibited virtually no sticking behavior whatsoever but the walkers tended to slip much more frequently and exhibited very little, if any, hinge-like motion. Chemotactic motion was observed when the walkers were put on a random walk path and they drifted toward high density regions. This directed motion was even observed when the walkers were placed on a longer random walk path. Additionally, a drift velocity was extracted from the "back-and-forth" path protocol. The drift velocity was larger for walkers caught in the drift current carrying them toward the 0μm region due to the gradient being larger in this direction; since the density of binding sites is greater in the 0μm region than in the 800μm region. This illustrated that we had successfully created the first synthetic chemotactic system.

Chapter 5: Conclusions and Future Work

In summary, we have created an experimental set-up that utilizes a rotating magnetic field that once actuated, induces magnetic beads to self-assemble and walk on surfaces. These walkers can be induced to move faster if the frequency increases and the more beads that compose a walker, the faster the velocity. We set out to create the first synthetic chemotactic system by utilizing the receptor-ligand pair of biotin-streptavidin. The presence of free biotin binding sites on the surface should, in theory, allow us to achieve directed motion as the walkers should move faster in areas with a high density of binding sites and slower in areas with a low density of binding sites. To create these gradients in binding sites, we placed a droplet of concentrated streptavidin on a slide and allowed the droplet to evaporate. We then conducted a series of continuous velocity runs across the sample in order to map the velocity profile of the sample. The velocity profiled illustrated regions with a high density of binding sites as well as a local minimum in the density of binding sites. We investigated this system further by analyzing the discrete motion of the walkers and confirmed the validity of our theoretical framework. We then placed the walkers on a random walk path and for the first time, synthetically obtained chemotactic directed motion as the walkers drifted towards high density regions. We also extracted a drift velocity for the walkers which confirmed our hypothesis that the 0μm region had a higher density of binding sites, and therefore gradient, than the 800μm region because the drift velocity was higher for walkers drifting towards the 0μm region.

There are a number of directions that this project can be taken in the future. A natural extension would be investigating new ligand-receptor pairs. For example, we could investigate an antigen-antibody pair using any one of the numerous kits available on the market today. These new ligand-receptor pairs would have a much lower binding affinity than streptavidin-biotin

pairs which means we could avoid these masking protocols and simply screen for different interaction strengths. Even more interesting would be to investigate how these different chemotactic systems could be tweaked by varying the temperature, pH, and salt concentrations. Any one of these parameters could vastly change the chemotactic system and yield untold new projects and applications. The move from in-vitro to in-vivo is promising as well. Haptotaxis, essentially chemotaxis in two dimensions, is prominent in white blood cells that firmly attach to and roll, translocating across the blood vessel walls in search of pathogens.[12] Reproducing this behavior with our walkers would transform the medical field.

Another future beneficial offshoot from this project could involve attempts to control fluid motion at the nanoscale in microfluidic devices. Microfluidic devices have garnered enormous interest in recent years, the goal being the creation of "labs-on-a-chip."[45-46] We could transform this field by controlling the flow and transport of fluids by utilizing carpets of our walkers, thereby creating complex hydrodynamic boundary conditions and patterns in the system. Such systems could allow for in-situ modifications, such as the solvent, and lends it to other characterization protocols that might require an open cell. Additionally, such systems wouldn't rely on a series of pumps and valves to control the flow. The decoupling of such systems from pumping devices makes the system amendable to use in other applications that pump required microfluidic devices wouldn't previously allow. And these walkers have already shown the capability to pump fluids in a desired direction.[29] These experiments would also allow us to test effective hydrodynamic interactions between arbitrary surfaces. Finally, this study of the transport of fluids at the nanoscale could allow us to synthetically mimic, using the knowledge obtained from the single walker experiments, how cilia moves mucus out of our lungs and

dictates embryo development.[47-49] The possible applications are virtually infinite and the potential of this field definitely has a bright future.

References

1. Phillips, R., J. Kondev and J. Theriot, *Physical Biology of the Cell.* 2009, New York: Garland Science. xxiv, 807 p.
2. Nelson, P.C., M. Radosavljević and S. Bromberg, *Biological Physics: Energy, Information, Life.*2004, New York: W.H. Freeman and Co. xxvi, 598 p.
3. Adler, J., *Chemotaxis in Bacteria.* Science, 1966. **153**(3737): p. 708-&.
4. Ridley, A.J., M.A. Schwartz, K. Burridge, R.A. Firtel, M.H. Ginsberg, G. Borisy, J.T. Parsons and A.R. Horwitz, *Cell migration: Integrating signals from front to back.* Science, 2003. **302**(5651): p. 1704-1709.
5. Berg, H.C., *Chemotaxis in Bacteria.* Annual Review of Biophysics and Bioengineering, 1975. **4**: p. 119-136.
6. Berg, H.C., *Bacterial Chemotaxis.* Bulletin of the American Physical Society, 1978. **23**(3): p. 221-221.
7. Berg, H.C., *Bacterial Chemotaxis.* Biophysical Journal, 1978. **21**(3): p. A29-A29.
8. Berg, H.C., *A Physicist Looks at Bacterial Chemotaxis.* Cold Spring Harbor Symposia on Quantitative Biology, 1988. **53**: p. 1-9.
9. Berg, H.C., *Chemotaxis and motility in Escherichia coli.* Journal of General Physiology, 2006. **128**(1).
10. Berg, H.C. and D.A. Brown, *Chemotaxis in Escherichia-Coli Analyzed by 3-Dimensional Tracking.* Nature, 1972. **239**(5374): p. 500-&.
11. Shiba, K., S.A. Baba, T. Inoue, and M. Yoshida, *Ca^{2+} burst occur around a local minimal concentration of attractant and trigger sperm chemotactic response.* Proceedings of the Natinoal Acadmey of Sciences of the United States of America, 2008. **107**(49): p. 19312-19317.
12. Jeon, N.L., H. Baskaran, S.K.W. Dertinger, G.M. Whitesides, L. Van de Water and M. Toner, *Neutrophil chemotaxis in linear and complex gradients of interleukin-8 formed in a microfabricated device.* Nature Biotechnology, 2002. **20**(8): p. 826-830.
13. Bizios, R., L. Lai, J.W. Fenton and A.B. Malik, *Thrombin-Induced Chemotaxis and Aggregation of Neutrophils.* Journal of Cellular Physiology, 1986. **128**(3): p. 485-490.
14. Rot, A., *Endothelial-Cell Binding of Nap-1/Il-8 - Role in Neutrophil Emigration.* Immunology Today, 1992. **13**(8): p. 291-294.
15. Rot, A., *Neutrophil Attractant Activation Protein-1 (Interleukin-8) Induces Invitro Neutrophil Migration by Haptotactic Mechanism.* European Journal of Immunology, 1993. **23**(1): p. 303-306.
16. Holmberg, A., Blomstergren, A., Nord, O., Lukacs, M., Lundeberg J., M. Uhlen, *The biotin-streptavidin interaction can be reversibly broken using water at eleveated temperatures.* Electrophoresis, 2005. **26**(3): p. 501-510.
17. Abbott, J.J., Peyer, K.E., Lagomarsino, M.C., Zhang, L., Dong, L., Kaliakatsos, I.K., B.J. Nelson, *How Should Microrobots Swim?* International Journal of Robotics Research,2009. **28**(11-12): p. 1434–1447.

18. Ebbens, S.J. and J.R. Howse, *In pursuit of propulsion at the nanoscale.* Soft Matter, 2010. **6**(4): p. 726-738.
19. Dreyfus, R., J. Baudry, M.L. Roper, M. Fermigier, H.A. Stone and J. Bibette, *Microscopic artificial swimmers.* Nature, 2005. **437**(7060): p. 862-865.
20. Lauga, E. and T.R. Powers, *The hydrodynamics of swimming microorganisms.* Reports on Progress in Physics, 2009. **72**(9).
21. Pak, O.S., W. Gao, J. Wang and E. Lauga, *High-speed propulsion of flexible nanowire motors: Theory and experiments.* Soft Matter, 2011. **7**(18): p. 8169-8181.
22. Hosoi, A.E. and E. Lauga, *Mechanical Aspects of Biological Locomotion.* Experimental Mechanics, 2010. **50**(9): p. 1259-1261.
23. Yu, T.S., E. Lauga and A.E. Hosoi, *Experimental investigations of elastic tail propulsion at low Reynolds number.* Physics of Fluids, 2006. **18**(9).
24. Golestanian, R., T.B. Liverpool and A. Ajdari, *Designing phoretic micro- and nano-swimmers.* New Journal of Physics, 2007. **9**.
25. Golestanian, R., *Synthetic Mechanochemical Molecular Swimmer.* Physical Review Letters, 2010. **105**(1).
26. Howse, J.R., R.A.L. Jones, A.J. Ryan, T. Gough, R. Vafabakhsh and R. Golestanian, *Self-motile colloidal particles: From directed propulsion to random walk.* Physical Review Letters, 2007. **99**(4).
27. Sabass, B. and U. Seifert, *Efficiency of Surface-Driven Motion: Nanoswimmers Beat Microswimmers.* Physical Review Letters, 2010. **105**(21)
28. Kosa, G., Jakab, P., Hata, N., Jolesz, F., Neubach, Z., Shoham, M., Zaaroor, M., G. Szekely, *Flagellar Swimming for Medical Micro Robots: Theory, Experiments and Application.* Biomedical Robotics and Biomechatronics, 2008. p.258-263
29. Alexander-Katz, A., C.E. Sing, L. Schmid, M.F. Schneider and T. Franke, *Controlled surface-induced flows from the motion of self-assembled colloidal walkers.* Proceedings of the National Academy of Sciences of the United States of America, 2010. **107**(2): p. 535-540.
30. Tierno, P., O. Guell, F. Sagues, R. Golestanian and I. Pagonabarraga, *Controlled propulsion in viscous fluids of magnetically actuated colloidal doublets.* Physical Review E, 2010. **81**(1).
31. Tierno, P., R. Golestanian, I. Pagonabarraga and F. Sagues, *Magnetically Actuated Colloidal Microswimmers.* Journal of Physical Chemistry B, 2008. **112**(51): p. 16525-16528.
32. Tierno, P., R. Golestanian, I. Pagonabarraga and F. Sagues, *Controlled Swimming in Confined Fluids of Magnetically Actuated Colloidal Rotors.* Physical Review Letters, 2008. **101**(21).
33. Morimoto, H., T. Ukai, Y. Nagaoka, N. Grobert and T. Maekawa, *Tumbling motion of magnetic particles on a magnetic substrate induced by a rotational magnetic field.* Physical Review E, 2008. **78**(2).
34. Mair, L.O., B. Evans, A.R. Hall, J. Carpenter, A. Shields, K. Ford, M. Millard and R. Superfine, *Highly controllable near-surface swimming of magnetic Janus nanorods:*

application to payload capture and manipulation. Journal of Physics D-Applied Physics, 2011. **44**(12).
35. Sing, C.E., L. Schmid, M.F. Schneider, T. Franke and A. Alexander-Katz, *Controlled surface-induced flows from the motion of self-assembled colloidal walkers.* Proceedings of the National Academy of Sciences of the United States of America, 2010. **107**(2): p. 535-540.
36. Vilfan, A. and F. Julicher, *Hydrodynamic flow patterns and synchronization of beating cilia.* Physical Review Letters, 2006. **96**(5).
37. Guirao, B. and J.F. Joanny, *Spontaneous creation of macroscopic flow and metachronal waves in an array of cilia.* Biophysical Journal, 2007. **92**(6): p. 1900-1917.
38. den Toonder, J., F. Bos, D. Broer, L. Filippini, M. Gillies, J. de Goede, T. Mol, M. Reijme, W. Talen, H. Wilderbeek, V. Khatavkar and P. Anderson, *Artificial cilia for active micro-fluidic mixing.* Lab on a Chip, 2008. **8**(4): p. 533-541.
39. Vilfan, M., A. Potocnik, B. Kavcic, N. Osterman, I. Poberaj, A. Vilfan and D. Babic, *Self-assembled artificial cilia.* Proceedings of the National Academy of Sciences of the United States of America, 2010. **107**(5): p. 1844-1847.
40. Florin, E.L., Moy, V.T., H.E. Gaub, *Adhesion Forces between Individual Ligand-Receptor Pairs.* Science, 1994. 264-5157: p. 415.
41. Livnah, O., Bayer, E.A., Wilcheck, M., J.L. Sussman, *Three-dimensional structures of avidin and the avidin-biotin complex.* Proceedings of the National Acadmey of Sciences of the United States of America, 1993. **90**(11): p. 5076-5080.
42. Morgenthaler, S., C. Zink and N.D. Spencer, *Surface-chemical and -morphological gradients.* Soft Matter, 2008. **4**(3): p. 419-434.
43. Morgenthaler, S., S.W. Lee, S. Zurcher and N.D. Spencer, *A simple, reproducible approach to the preparation of surface-chemical gradients.* Langmuir, 2003. **19**(25): p. 10459-10462.
44. Genzer, J. and R.R. Bhat, *Surface-bound soft matter gradients.* Langmuir, 2008. **24**(6): p. 2294-2317.
45. Elman, N.M., H. Ben-Yoav, M. Sternheim, R. Rosen, S. Krylov and Y. Shacham-Diamand, *Towards toxicity detection using a lab-on-chip based on the integration of MOEMS and whole-cell sensors.* Biosensors & Bioelectronics, 2008. **23**(11): p. 1631-1636.
46. Evans, S., *Towards a true lab-on-a-chip system - On the right track.* Physical Chemistry Chemical Physics, 2004. **6**(7): p. C27-C27.
47. Knowles, M.R. and R.C. Boucher, *Mucus clearance as a primary innate defense mechanism for mammalian airways.* Journal of Clinical Investigation, 2002. **109**(5): p. 571-577.
48. Shields, A.R., B.L. Fiser, B.A. Evans, M.R. Falvo, S. Washburn and R. Superfine, *Biomimetic cilia arrays generate simultaneous pumping and mixing regimes.* Proceedings of the National Academy of Sciences of the United States of America, 2010. **107**(36): p. 15670-15675.

49. Cribb, J., S. Norris, P. Moore, M.G. Forest, J.K. Sheehan and R. Superfine, *Might Cilia Use Strain Thickening to Encourage Mucus Transport?* Pediatric Pulmonology, 2009: p. 264-264.
50. Fisher, J., R. Superfine, E.T. O'Brien, R.M. Taylor, C.W. Davis, H. Matsui, L. Vicci, G. Matthews and B. Wilde, *Motion and force generation of cilia in human lung cell cultures.* Biophysical Journal, 2003. **84**(2): p. 531A-531A.
51. Evans, B.A., A.R. Shields, R.L. Carroll, S. Washburn, M.R. Falvo and R. Superfine, *Magnetically actuated nanorod arrays as biomimetic cilia.* Nano Letters, 2007. **7**(5): p. 1428-1434.
52. Gast, A.P. Roberston, C.R., Wang, S.W., M.T., Yatcilla, *Two-dimensional streptavidin crystals: macropatterns and micro-organization.* Biomolecular Engineering, 1999. **16**(1-4): p. 21-27.
53. Kenkare, P.U., C.K. Hall, *Modeling of Phase Seperation in PEG-Salt Aqueous Two-Phase Systems.* Materials, Interfaces, and Electrochemical Phenomena, 1996. **42**(12): p. 3508-2522.

Acknowledgements

I would like to thank C.K. Umanchi for his help in running the VSM measurement which allowed us to accurately characterize the magnetic properties of our Solulink beads. Also, Stephanie Moran should be acknowledged for all the work she did to help get this project off the ground. Mike Tarkanian and David Bono also did an amazing job in helping to create our experimental apparatus and getting the walkers to first start moving. I'd also like to recognize Tim McClure and the CMSE for all their help in trying to quantify the coverage of streptavidin on the surface of our biotin slides. A special thanks to Prabhani Atukorale and the Koch Institute for allowing us to use their confocal microscope to capture the coverage of streptavidin using fluorescent labels, and to Professor Olsen for his continuous help throughout this project in solving all of our chemistry problems whenever they would come up.

I would also like to thank the numerous contributions made by all the member of the Alexander-Katz Group: Charles Sing, Reid Van Lehn, YJ, Hseih, and Yvonne. They were always readily available to help with any experiments and the insights gained from discussing experimental data really helped in understanding the system.

Finally, Professor Alexander-Katz. I was honored to be given the opportunity to work on this project. His enthusiasm and energy made all the work enjoyable and continues to spur me forward. More importantly, his support and belief in not only me, but all of his other students, really creates the best work/research environment that I've ever had the privilege to be a part of anywhere. However, the most impressive aspect of working for Professor Alexander-Katz is that he is always free to meet and discuss even the smaller updates on a particular project or experiment. In fact, he actually encourages frequent updates, meetings, and discussions about what's happening and the next steps to take. If it wasn't for these frequent meetings, advice on the next experiment to run, and even help in running some experiments, this project would never have gotten this far. Although I know I'll never be able to adequately repay Professor Alexander-Katz for everything he has done for me, I will continue to work as hard as I possibly can to contribute to the success of the Alexander-Katz group.

Appendix: Frequency and Walk Duration Effect on Chemotactic System

The binding potential of the biotin-streptavidin ligand-receptor pair can be manipulated by a number of the variables in our system, including frequency. To get a quick diagnostic test of the chemotactic system a quick "back-and-forth" protocol was employed for 100 coin flips for a two bead walker placed at approximately 700μm. The frequency was set to 5Hz and the duration of the walk was approximately 2 seconds. The distance traveled and subsequent velocity was analyzed in Mathematica and then a histogram was generated from the data as seen in Figures 24 and 25.

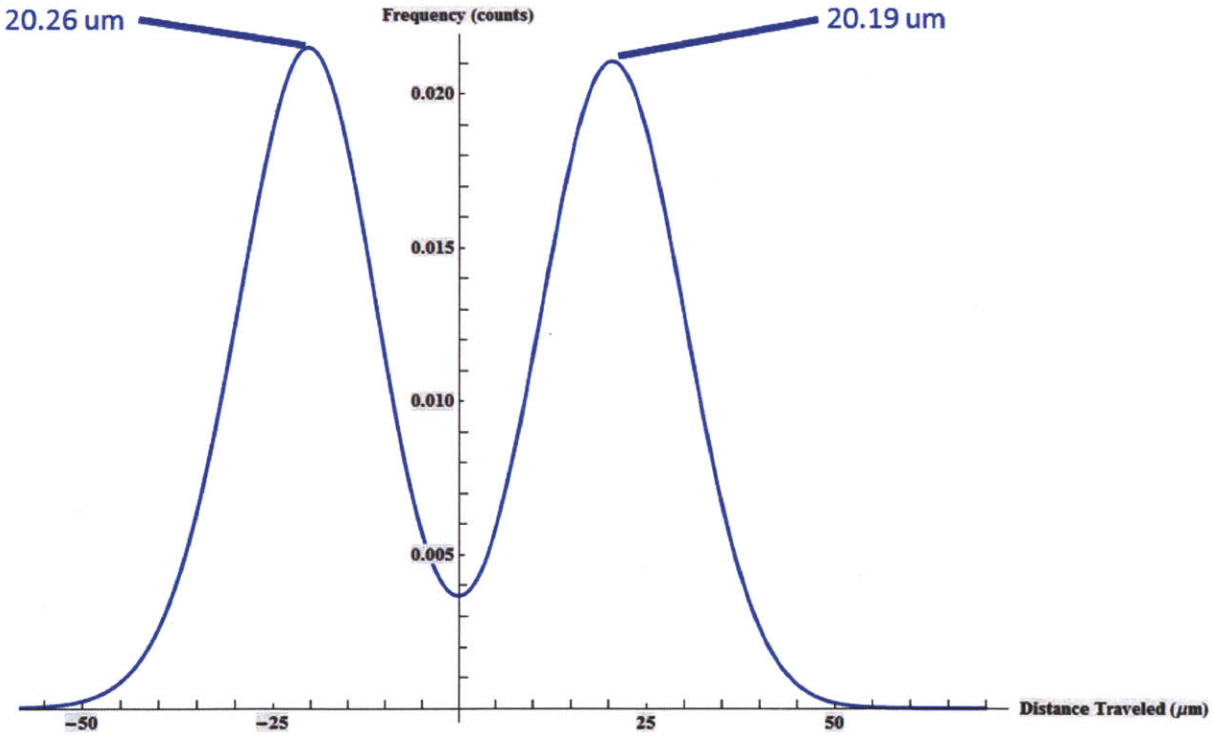

Figure 24: The distance traveled at 5Hz for walkers starting from approximately 700μm is virtually identical forward and backward. When the walkers were operated at 1Hz, we observed a discernible difference in distance traveled when traversing forward and backward in the 700μm region. The frequency is having some effect that is suppressing the effect of the binding potential of the biotin-streptavidin ligand-receptor pair.

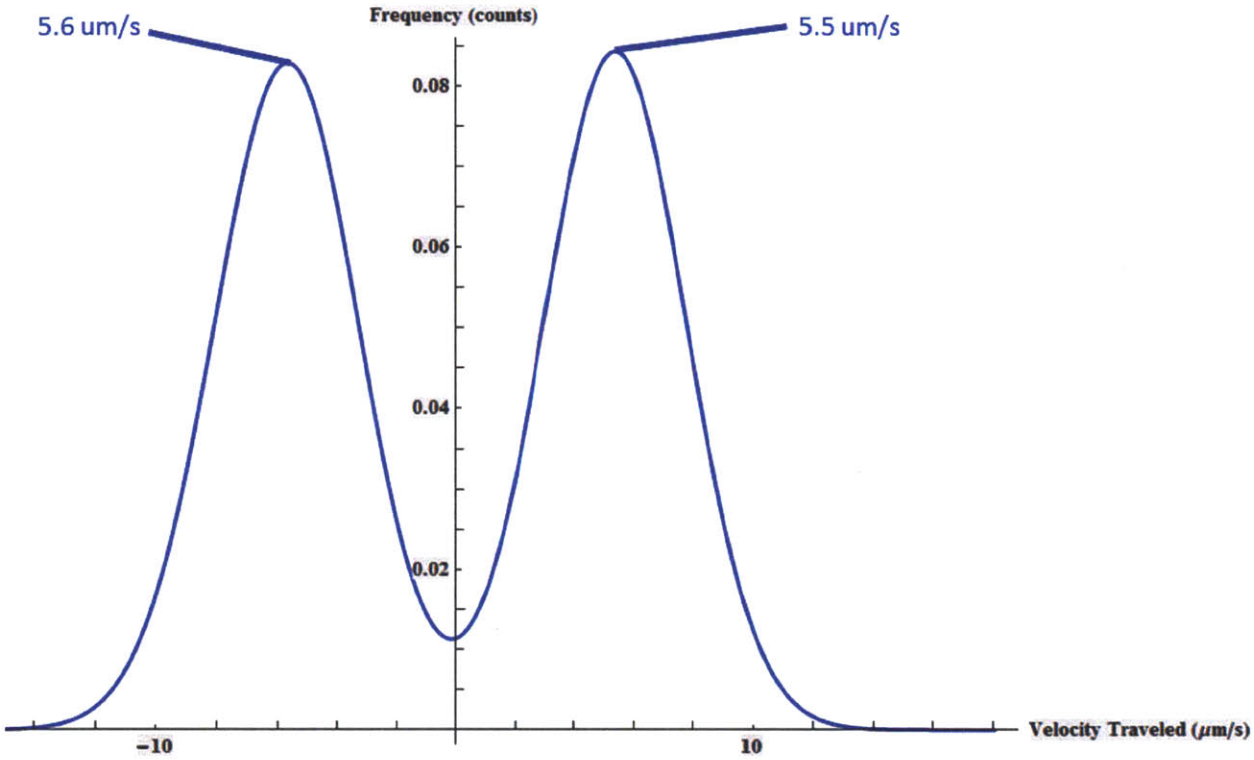

Figure 25: The velocity for walkers operated at 5Hz is similarly virtually identical when the walkers are moved forward and backwards.

Interestingly, it seems that at 5Hz the walkers are able to overcome the chemotactic pull of the system, as the velocity and distance traveled is virtually identical regardless of the direction of motion. This behavior might be due to the frequency of turning being so rapid that the walker is turning faster than the binding kinetics of the biotin-streptavidin pair. Thus, the walkers at this frequency and higher don't seem to "feel" the drift or chemotactic pull.

We also wanted to see the effect that increasing the "walking time" of each coin flip had on the chemotactic system. Using the same "short" random walk protocol previously described, we simply increased the walking time for each coin flip to 10 and 20 seconds. Position data was collected in the usual manner and the various histogram plots were generated as seen in Figure 26.

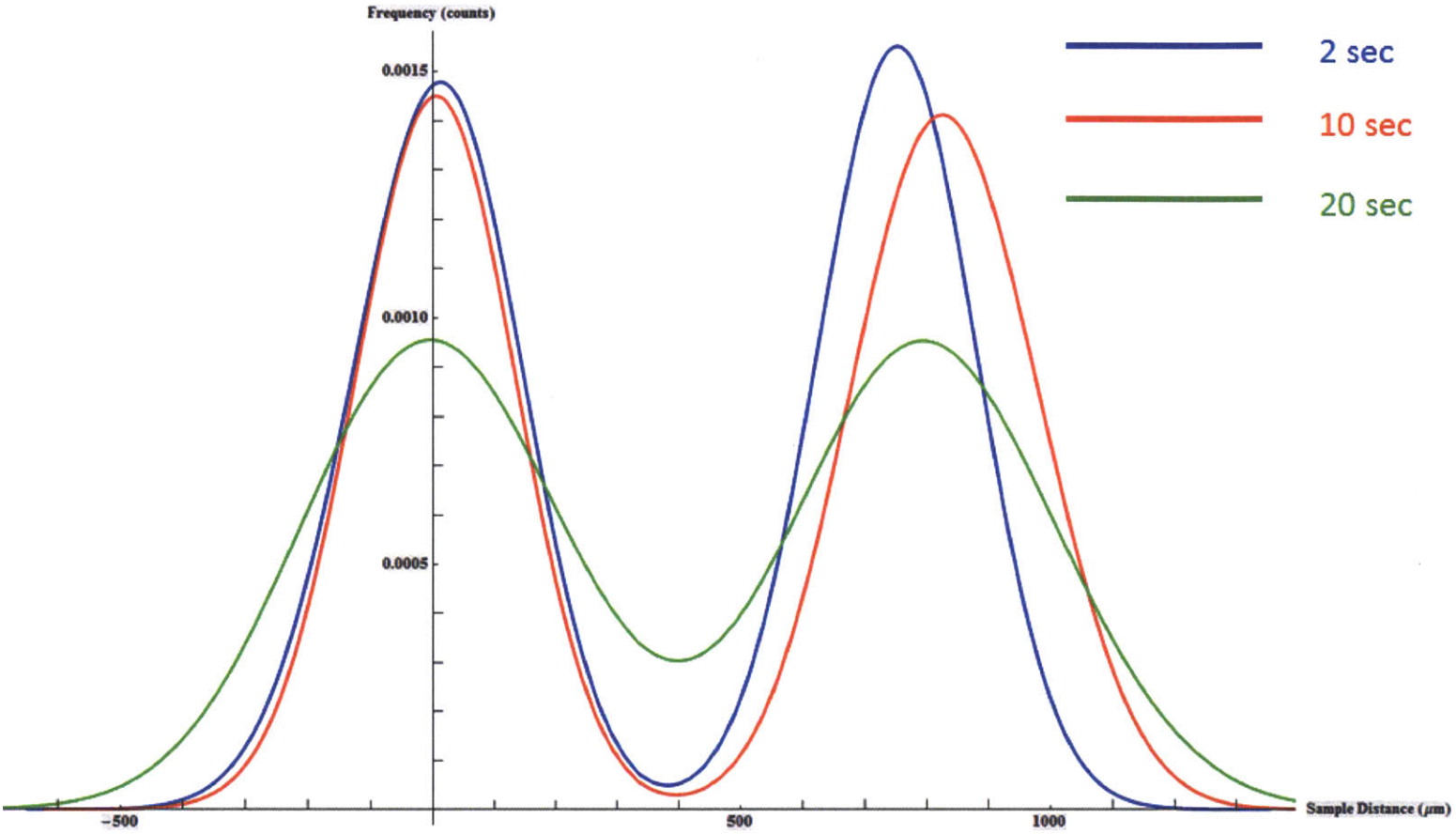

Figure 26: As the time that the walkers are given to transverse per coin toss increases, we see this diffusive flattening of the walker histograms. The increased walking time increases the probability that the walker will walk out of each respective "potential well." However, even at these long walking times the chemotactic effect is still seen, a testament to the biotin-streptavidin receptor-ligand pair.

This data is much more consistent with our theoretical understanding as the histogram curves should tend to flatten as the duration of the walk is increased. Increasing the walking time will increase the probability that the walkers can access new states as well as increasing the probability that the walkers can leave the "potential well" when in a high density area. However, it should be noted how strong this chemotactic effect is. Even when the walk duration is increased tenfold, there is still significant aggregation in high density areas.

Appendix: Gradient Quantification

The next crucial step in this project is the quantification of streptavidin coverage on the sample. Once this is done, we can start to generate theoretical simulations to model our experimental results in order to get a deeper fundamental understanding of this chemotactic directed motion. A number of experimental techniques have been attempted in order to extrapolate the streptavidin coverage, aside from the velocity measurements, including AFM and profilometer measurements, all of which have met with inconclusive results. However, we are beginning to see some tangible results with confocal microscopy characterization. We purchased fluorescently labeled streptavidin (Alexa Fluora) and excited the streptavidin with a 488nm laser. Images were taken to characterize the relative coverage as seen in Figure 27.

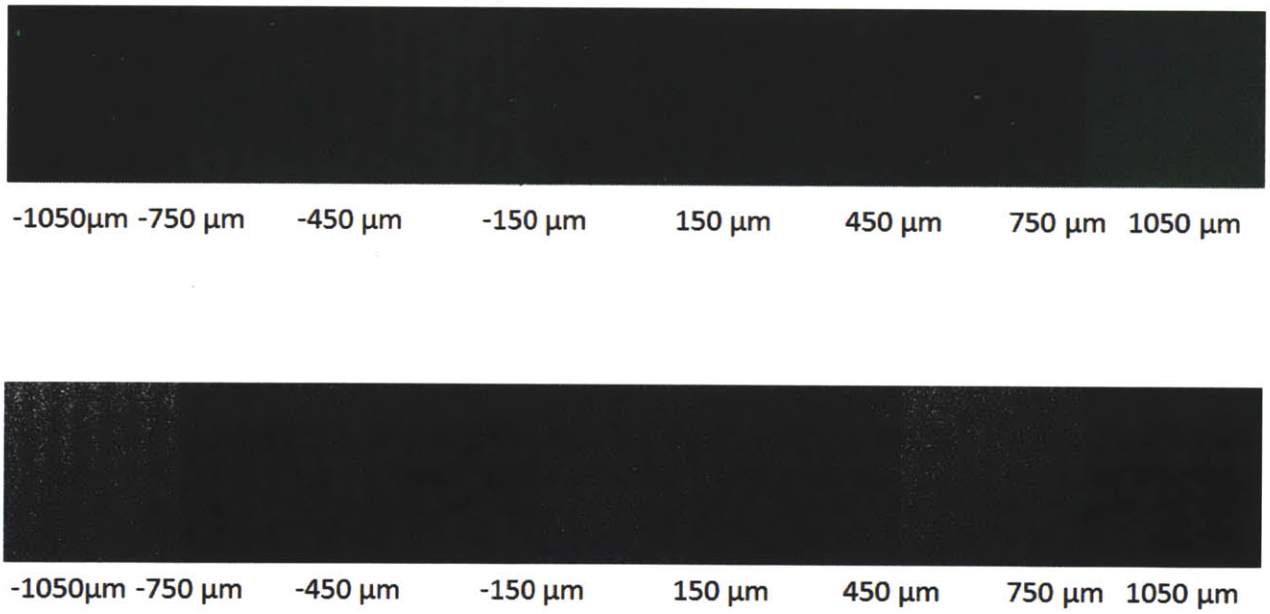

Figure 27: The top panel images are confocal microscopy images that span the entire streptavidin droplet. The darker regions correspond to a higher density of binding sites while brighter regions indicate streptavidin coverage. The bottom panel is a mathematica contour plot that was generated from the confocal microscope images. The white spots correspond to free binding sites while dark spots indicate a covered binding site.

A more thorough protocol needs to be generated in order to get a baseline and then we can get actual quantitative results as to streptavidin coverage. However, even in this cursory experiment,

our previous experimentally justified hypothesis that at 0 and 800μm there is a high density of binding sites appears to be true. Looking at the top panel, we see dark spots which correlate to free binding sites, at around 0 and 800μm while we see brighter regions, corresponding to a lower density of free binding sites, near 450μm as expected. The bottom panel, showing contour plots of the previous images, confirms this observation.

Appendix: Dendritic Formation

During our attempts to characterize the streptavidin surface coverage via AFM and profilometer test, we took a look at the sample residue which is something we had yet to do due to the cleaning protocol involved before the channel is created. Amazingly, we saw dendritic crystallization formations carpeting the surface of the sample. As seen in Figure 28, these dendritic formations span the entire sample, save the edge of the droplet where the red fluorescent streptavidin accumulated (also ignore the red line on some of the pictures, this is just a scale bar measurement).

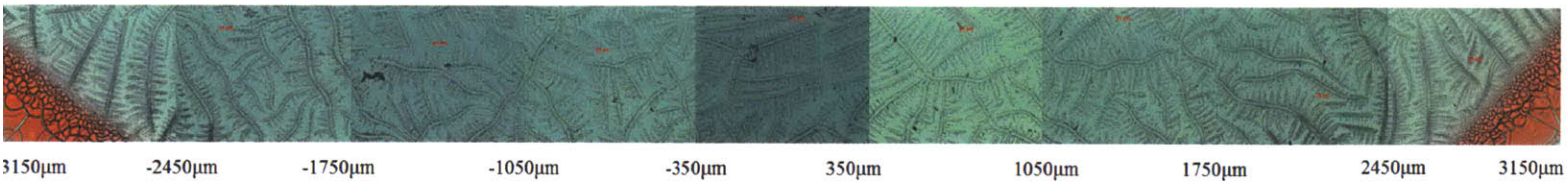

Figure 28: Image of the excess streptavidin crystallization into dendritic formations. These formations span the entire sample with many of the dendrites having multiple branches.

Streptavidin has previously been shown to crystallize in such dendritic formations.[52] These formations would be of greater concern as they would have obstruct walker motion and negated our previous results. However, the rigorous cleaning protocol removes these dendritic formations assuring that any directed motion was chemotactic, not due to dendritic formation topology.

Appendix: Effect of Temperature and Salt Concentration on PEG Phase Transition

In thinking about masking protocols and how to determine the optimal PEG coverage of our walkers in our chemotactic system, we also had to consider PEG phase separation when PEG is in salt-water systems. PEG-water-salt systems have been thoroughly investigated in previous works and interestingly in PEG-water-salt systems, PEG exhibits a phase transition depending on the concentration of salt.[53] As seen in the phase diagram in Figure 29, PEG exhibits a LCST and UCST that is modulated by the concentration of salt and PEG molecular weight.

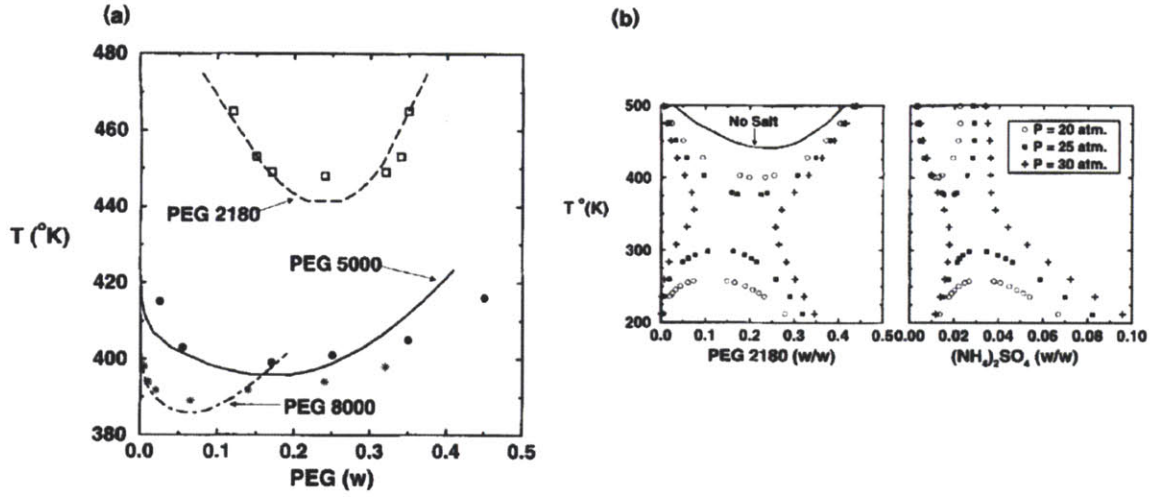

Figure 19: a) Theoretical and experimental phase diagrams for a PEG-water mixture. b) Theoretical phase diagrams for a PEG-water-salt mixture.[53]

This phase separation is due to a number of interactions occurring in this system including coulombic, hydrogen bonding, and Yukawa attractions. This poses a critical problem for our system since the presence of salt induces this PEG phase transition which drastically weakens PEG's ability to mask the biotin-streptavidin interaction by reducing the binding interaction potential. This effect was observed experimentally as the presence of any salt buffer eliminated walker motion. To negate this effect and avoid PEG phase separation, we worked solely with aqueous solutions when PEG was utilized in experiments, avoiding these phase transitions.